博士論文

Nonlinear Phenomena in Ion Acoustic Waves: Transition from Soliton to Chaos and Bifurcation of Sheath Structure

（イオン音波の非線形現象：ソリトンからカオスへの遷移
およびシース構造の分岐）

大野 裕司

Doctorial Dissertation

Nonlinear Phenomena in Ion Acoustic Waves: Transition from Soliton to Chaos and Bifurcation of Sheath Structure

Yuji Ohno

Department of Advanced Energy
Graduate School of Frontier Sciences
The University of Tokyo

March 2017

Contents

List of Figures

List of Tables

Chapter 1

Introduction

Nonlinearity invokes interactions among different scales and produces various structures from order to chaos. A typical example, in which order and chaos coexist, is the *wave* in the theory of fields. Especially, in plasma physics, collective motions and electromagnetic fields produce waves. Particles composing plasmas interact via microscopic electromagnetic forces, but the forces reach to long ranges and produce collective motions of plasmas. Simultaneously, the collective motions produce macroscopic electromagnetic fields. Thus collective motions of plasma cause "strong" nonlinearities.

The *Ion acoustic wave* is a longitudinal wave produced by the collective electric fields. In the ion acoustic waves, the combination of the nonlinearity (by fluid convection) and the dispersion (by non-local electric interactions) produces both aspects of nonlinear structures—order and chaos.

In this dissertation, we focus on two nonlinear ordered structures in ion acoustic waves—*soliton* and *electrostatic sheath*.[1)] The soliton is a solitary wave which propagates without changing its shape and velocity during collisions with other solitons. The solitons are also featured by that the evolution equations are *integrable*. The electrostatic sheath is a steady steep structure of electrostatic potential. It may also

[1)] We do not include the terms of magnetic fields, but it does not mean that we ignore magnetic fields. We may consider that waves propagate along the magnetic fields and the Lorenz force $\boldsymbol{v} \times \boldsymbol{B}$ disappears.

be seen as a standing shock of the ion acoustic wave.

In this chapter, we review studies of ion acoustic waves—focusing on soliton and electrostatic sheath—and state the objective of the dissertation. In Section 1.1, we review works on ion acoustic solitons, especially focusing on derivations of soliton equations. In Section 1.2, we describe mathematical theories of solitons. We also elucidate that the Kadomtsev–Petviashvili equation, a two-dimensional soliton equation, is an archetype of soliton equations. When the integrability disappears, chaos may occur. We review studies of non-integrability and transition from soliton to chaos in Section 1.3. In Section 1.4, we introduce a recently formulated equation, a generalized Kadomtsev–Petviashvili equation, that takes into account vortex. The analysis of the equation is the first objective of the dissertation. We move to introduce the studies of the electrostatic sheath. In Section 1.5, we review the first theoretical treatment of the sheath by Bohm and related works. In Section 1.6, we propose an idea to associate sheath structure with a thermodynamical context and review some related works. Finally, we will describe the plan of the dissertation in Section 1.7.

1.1 Nonlinear ion acoustic waves and soliton equations: KdV equation and KP equation

Theoretical studies of ion acoustic solitons started by the derivation of the Korteweg–de Vries (KdV) equation (the one-dimensional soliton equation)

$$\frac{\partial u}{\partial t} + \alpha u \frac{\partial u}{\partial x} + \beta \frac{\partial^3 u}{\partial x^3} = 0, \tag{1.1}$$

which Washimi and Taniuti [81] found. They derived the equation from ion acoustic wave equations by the *reductive perturbation method*. This foundation indicates that small amplitude ion acoustic waves become solitons in the one-dimensional flat geometry. The second term of the KdV equation (1.1)—a nonlinear convection—produces wave steepening, and the third term—a third-order derivative—brings about disper-

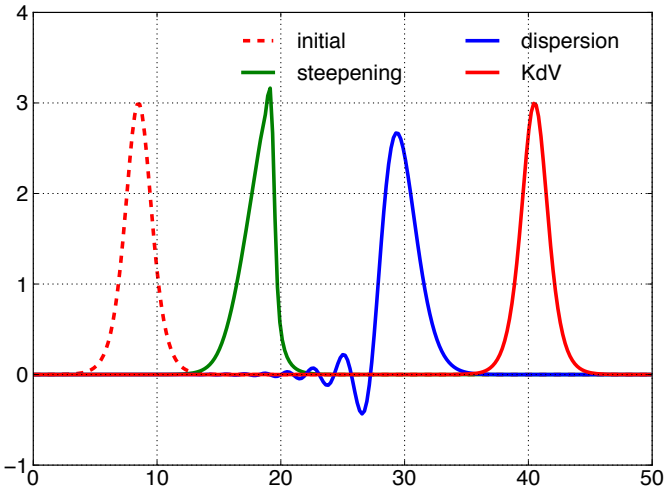

Figure 1.1: Comparison of wave steepening and dispersion; these effects balance in the KdV equation (horizontal locations adjusted for visibility)

sion. The reductive perturbation method deriving the KdV equation consider a scale where these effects balance [86] and a solitary wave propagates without changing its shape (see Figure 1.1).

After this work, several directions of generalizations have been studied. For example, Tappert [73] and Tagare [70] derived the KdV equation with modified coefficients α, β from the ion acoustic wave system including an ion temperature. The effects of multi-ions [79] and dust plasmas [75] were also studied. The modified KdV equation, including a third-order nonlinear term as

$$\frac{\partial u}{\partial t} + \alpha u^2 \frac{\partial u}{\partial x} + \beta \frac{\partial^3 u}{\partial x^3} = 0, \tag{1.2}$$

is also a soliton equation. For ion acoustic waves, these equations are derived considering trapped electrons [66], three-waves interaction [39], and negative ions [33].

Another direction of generalization, increasing the spatial dimension, was studied by Kako and Rowlands [32]. They obtained three types of equations, including the two-dimensional Kadomtsev–Petviashvili (KP) equation

$$\frac{\partial}{\partial x}\left(\frac{\partial u}{\partial t} + \alpha u \frac{\partial u}{\partial x} + \beta \frac{\partial^3 u}{\partial x^3}\right) + \gamma \frac{\partial^2 u}{\partial y^2} = 0. \tag{1.3}$$

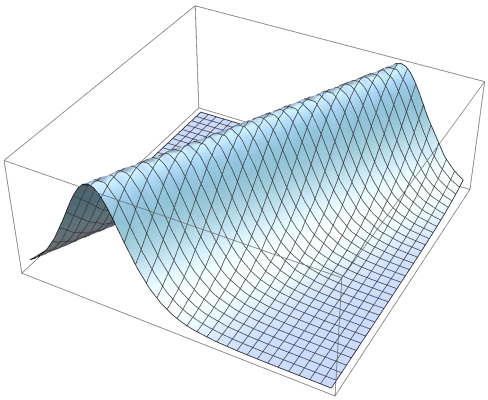

Figure 1.2: A line-soliton solution of the KP equation

The two-dimensional KP equation is also a soliton equation, and its soliton solution is called *line soliton* (Figure 1.2). In Section 2.1.1 we remember the derivation of the KdV and KP equations. Generalizations of the KP equation including effects of multi-ions [80], dust plasma [21], and multi-temperature [25, 45], are also investigated. The modified KP equation including a third-order term such as the modified KdV equation (1.2) was also derived [59].

Effects of higher-order terms in the reductive perturbation method have also been widely studied (see, e.g., Refs. [27, 40, 75] and references therein). The lowest order soliton is called a core part, higher order perturbations are called clouds, and the core solitons with clouds are called dressed solitons. Since the equations for clouds include inhomogeneous terms composed of the core, clouds arise from the zero initial condition.

Here we have introduced theoretical studies on ion acoustic soliton equations. We remark that ion acoustic (KdV and KP) solitons are experimentally observed (see review articles such as Refs. [47, 53, 78]). We also briefly address the discovery of the KdV equation and the KP equation. Boussinesq [9] firstly derived the KdV equation from the equation of shallow water waves. Korteweg and de Vries [41] re-derived the equation and obtained cnoidal wave solutions including solitary wave solutions. Kadomtsev and Petviashvili [31] constructed the two-dimensional KP equation by

considering a perturbation for the KdV equation. Their aim was to investigate the stability of the soliton solution of the KdV equation. The KP equation with $\alpha > 0, \beta > 0, \gamma > 0$ is called the KP-II equation, and that with $\alpha > 0, \beta > 0, \gamma < 0$ is called the KP-I equation.[2)] They showed that the soliton is stable in the KP-II equation and unstable in the KP-I equation.

1.2 Infinite-dimensional integrable system

In general, nonlinear partial differential equations are not integrable (solvable). The KdV equation and the two-dimensional KP equation belong to a special class, soliton equations, and they are integrable. There are some common properties of integrable systems, e.g., they have an infinite number of independent conserved quantities, they can be solved by the inverse scattering transform (IST) method, and they have the Painlevé property. In this section, we briefly review the IST method and see that the two-dimensional KP equation is an "archetype" of infinite-dimensional integrable systems. The method also may clarify the existence of an infinite number of independent conserved quantities. The Painlevé property is important in another sense since we can verify whether a given equation has Painlevé property or not by a certain procedure. (We will review the Painlevé property in Section 3.1 as a preparation for the application in Section 3.2.)

Soliton of the KdV equation was discovered and named by Zabusky and Kruskal [91]. They analyzed the KdV equation numerically and found that an initially sinusoidal wave splits into an array of solitary pulses and return to the initial state. Moreover, they found that each pulse propagates without changing its shape during collisions. Considering this property like a particle, they referred to the solitary waves as solitons.

A significant work of soliton theory was achieved by Gardner, Greene, Kruskal,

[2)] Here we consider that the signs of α and β are positive. We can change the signs by applying the transformation $u \mapsto -u$, $x \mapsto -x$, $t \mapsto -t$.

and Miura (GGKM) [24]—they discovered a solving method of the KdV equation. They found that when u obeys the KdV equation $\partial_t u - 6u\partial_x u + \partial_x^3 u = 0$, eigenvalues λ of the steady Schrödinger operator $-\partial_x^2 + u$ are conserved. Then, instead of considering the evolution of u (the KdV equation), we may consider the evolution of a "wave function" ψ. It was already known that u can be reconstructed from the scattering date of ψ (solving an inverse scattering problem). GGKM found that the evolution of ψ is easy to solve.

After the work of GGKM, Lax [44] formulated the IST method with the usage of linear operators. He introduced a pair of linear operators $L = -\partial_x^2 + u$ and $A = -4\partial_z^3 + 6u\partial_x + 3(\partial_x u)$ (called *Lax pair*) and expressed the eigenvalue problem as $L\psi = \lambda\psi$ and the evolution of ψ as $\partial_t \psi = A\psi$. Since this system is overdetermined, the compatibility condition must be satisfied. The condition is $\partial_t L = [A, L]$, called the Lax equation, which is identical to the KdV equation. Lax's formulation opened the way to apply the IST method for other equations. For example, Dryuma [20] introduced the Lax pair for the two-dimensional KP equation, and Zakharov and Shabat [94] solved the equation by the IST method. We note that the L operator for the two-dimensional KP equation is *not* the two-dimensional Schrödinger operator, but the non-steady Schrödinger operator, where y is the "time."

Soliton equations, such as the KdV equation and the two-dimensional KP equation, are solved with the IST method. The IST method also provides *action-angle pairs* for soliton equations. In the theory of finite-dimensional system, an integrable system (in the sense of Liouville) has a canonical transformation to an action-angle pair [6]. Zakharov and Faddeev [92] proved that the scattering data configures an action-angle pair of the KdV equation. Lipovskii [46] found that a similar relation is also valid for the two-dimensional KP-II equation.

A breakthrough in soliton theory—geometrical structures of the two-dimensional KP equation—was discovered by Sato [65] and his pupils, called "Kyoto School." In the Sato theory, we consider the Lax pair with the pseudo-differential operator and

construct a hierarchy of an infinite number of functions and variables. We obtain the two-dimensional KP equation as the simplest nontrivial equation, and thus the hierarchy is called the KP hierarchy. Many soliton equations, such as the KdV equation, the Boussinesq equation, and the coupled KdV equation, are obtained from the KP hierarchy. Thus, we can view the two-dimensional KP equation as an archetype of soliton equations. We give a brief introduction to Sato theory in Appendix A.2. For details of the Sato theory, see review articles [17, 58] or books [19, 50].

1.3 Non-integrable system: transition from soliton to chaos

Integrability is built upon a delicate balance of terms in an evolution equation. As described in Section 1.1, the integrability of the KdV equation is due to the balance between wave steepening by the nonlinear convective term and wave dispersion by the third-order differential term. In many cases, additional effects, such as forces and variable coefficients, disrupt the balances. For example, although both of the KdV equation (1.1) and the viscous Burgers equation

$$\frac{\partial u}{\partial t} + \alpha u \frac{\partial u}{\partial x} + \nu \frac{\partial^2 u}{\partial x^2} = 0 \tag{1.4}$$

are integrable, the KdV–Burgers equation

$$\frac{\partial u}{\partial t} + \alpha u \frac{\partial u}{\partial x} + \nu \frac{\partial^2 u}{\partial x^2} + \beta \frac{\partial^3 u}{\partial x^3} = 0 \tag{1.5}$$

is *not* integrable [26]. We give another example; a generalized two-dimensional KP equation with variable coefficients

$$\begin{aligned} &\frac{\partial}{\partial x}\left[\frac{\partial u}{\partial t} + h_1(y,t)\frac{\partial^3 u}{\partial x^3} + h_2(y,t)u\frac{\partial u}{\partial x}\right] \\ &+ h_3(y,t)\frac{\partial^2 u}{\partial x^2} + h_4(y,t)\frac{\partial^2 u}{\partial x \partial y} + h_5(y,t)\frac{\partial^2 u}{\partial y^2} + h_6(y,t)\frac{\partial u}{\partial x} + h_7(y,t)\frac{\partial u}{\partial y} = 0 \end{aligned} \tag{1.6}$$

is integrable only when the constraints for coefficients

$$\begin{aligned} &h_2 = \alpha h_1 \exp\left(\int h_6 \,\mathrm{d}t\right), \qquad \frac{\partial h_4}{\partial y} = h_6 + \frac{\partial}{\partial t}\ln(h_1/h_2), \\ &h_5 = 3\beta^2 h_1, \qquad \frac{\partial h_1}{\partial y} = \frac{\partial h_2}{\partial y} = h_7 = 0 \qquad (\alpha, \beta = \text{const.}). \end{aligned} \tag{1.7}$$

are satisfied [74].

Another generalization bringing about a non-integrability is increasing the spatial dimension. In fact, there are few integrable equations in the three-dimensional space. For example, the three-dimensional KP equation

$$\frac{\partial}{\partial x}\left(\frac{\partial u}{\partial t} + \alpha u\frac{\partial u}{\partial x} + \beta\frac{\partial^3 u}{\partial x^3}\right) + \gamma\frac{\partial^2 u}{\partial y^2} + \delta\frac{\partial^2 u}{\partial z^2} = 0 \tag{1.8}$$

is not integrable [11, 48, 63]. Although Ruan, Low, and Chen [63] produced integrable three-dimensional systems from the three-dimensional KP equation, the obtained models represent only approximations of the original KP equation.

When an integrability disappears, we consider that chaos may occur. For finite-dimensional slightly perturbed Hamiltonian systems, a well-known theory called Kolmogorov–Arnold–Moser (KAM) theory [6, 10] guarantees the stability (the existence of invariant tori). Perturbations on infinite-dimensional integrable systems have also been studied. For example, Nozaki and Bekki [56] analyzed the nonlinear Schrödinger (NLS) equation[3)]

$$\mathrm{i}\frac{\partial q}{\partial t} + \frac{\partial^2 q}{\partial x^2} + 2|q|^2 q = 0, \tag{1.9}$$

including periodic external forces and dissipation terms (q is a complex function and i is the imaginary unit). They derived a finite-dimensional system by considering perturbations in parameters of soliton solutions. They showed that the transition from soliton to chaos occurs depending on strengths of the external forces in both of the original infinite-dimensional system and reduced finite-dimensional system. Subsequently, Nozaki [55] analyzed a perturbed NLS equation (slightly different from that of Ref. [56]) and showed that stabilities of perturbed solitons are explained in terms of the KAM theory.

[3)] The NLS equation is a soliton equation (the Lax pair was found by Zakharov and Shabat [93]).

1.4 Ion acoustic wave propagating in vortex: Kadomtsev–Petviashvili–Yoshida equation

As referred in Section 1.1, many studies have generalized the KdV equation and KP equation for ion acoustic waves including physical effects. However, few works have focused on *vortex*. From the perspective of topological constraints of fluid dynamics, fluid flows without vorticities reside in a singular manifold embedded in a larger phase space [89] (see also Appendix A.3).

Recently, Yoshida proposed a generalization of the KP equation including vortex:

$$\frac{\partial}{\partial x}\left(\frac{\partial u}{\partial t}+u\frac{\partial u}{\partial x}+\frac{1}{2}\frac{\partial^3 u}{\partial x^3}+[u,\psi]\right)+\frac{1}{2}\Delta_\perp u=0, \tag{1.10}$$

$$\frac{\partial}{\partial t}\Delta_\perp\psi+[\Delta\psi,\psi]=0. \tag{1.11}$$

The first equation is a generalization of the three-dimensional KP equation with the convective term $[u,\psi]=\partial_y u\partial_z\psi-\partial_z u\partial_y\psi$. The second equation is the two-dimensional Euler vorticity equation for the additional field ψ. We call the system of equations *Kadomtsev–Petviashvili–Yoshida (KPY) equations*. As written in Section 1.2, the KP equation is an archetype of soliton equations. The KPY equation describes a minimal departure from the equation to including vortex.

Applying Helmholtz's theorem, we may decompose a three-dimensional vector field vanishing at infinity into two components: compressible (rotation-free) and vortical (divergence-free) ones.[4)] The compressible component is rotation-free and produces longitudinal waves, and the vortical component is divergence-free and produces transverse waves. In many cases, we consider one of these components—typical example of the former is the ion acoustic wave, and the latter is the Euler equation. The KPY equations describe a coupling of the two components (Table 1.1).

Analyzing the properties of the KPY equation is the first objective of the dissertation. We will also review the derivation in Section 2.2 with a detailed explanation

[4)] If we consider an unbounded region or a field non-vanishing at infinity, we have to add a harmonic field (divergence-free and rotation-free) component. This decomposition is called the Helmholtz–Hodge decomposition.

Table 1.1: Classification of velocity component and characterization of a new system (KPY equation). The compressible part is rotation-free and its wave is longitudinal, and the vortical part is divergence-free and its wave is transverse. A typical example of the former is the ion acoustic wave, and that of the latter is the Euler equation. The KPY equations are the coupling of the KP equation (ion acoustic wave) and the Euler vorticity equation.

	compressible	vortical
divergence	$\nabla \cdot \boldsymbol{u} \neq 0$	$\nabla \cdot \boldsymbol{u} = 0$
rotation	$\nabla \times \boldsymbol{u} = 0$	$\nabla \times \boldsymbol{u} \neq 0$
wave	longitudinal $\boldsymbol{k} \times \boldsymbol{u} = 0$	transverse $\boldsymbol{k} \cdot \boldsymbol{u} = 0$
example	ion acoustic wave (KdV/KP)	Euler
	$\rightarrow$ KPY	

of the meaning of generalization.

1.5 Electrostatic sheath: steady structure created between plasma and wall

Now we move to reviewing works on electrostatic sheaths. The sheath arises around a wall. The phenomenological explanation of sheath is as following [12]. Ions and electrons in plasmas hit the wall and disappear by recombination. Since electrons have larger thermal velocity than ions, electrons disappear rapidly. Thus the ion density is greater than the electron density around the wall, and the plasma has a positive electrostatic potential compared to the wall. This potential gradient cannot become thicker than several times of the Debye length $\lambda_{\mathrm{D}} = \sqrt{\varepsilon_0 T_{\mathrm{e}}/n_0 e^2}$ because of the Debye shielding.

The pioneer work of sheath is that by Langmuir [43]. He observed that the ion velocity passing the sheath region have to be a certain value. Bohm [8] studied the

sheath theoretically and obtained the equation called *Bohm equation*:

$$\frac{\mathrm{d}^2\varphi}{\mathrm{d}x^2} = \mathrm{e}^{\varphi} - \left(1 - \frac{2\varphi}{\mathcal{M}^2}\right)^{-1/2}, \tag{1.12}$$

where $\mathcal{M} = u_0/\sqrt{T_\mathrm{e}/m}$ is the ion velocity at the entrance of the sheath normalized with the ion sound speed $\sqrt{T_\mathrm{e}/m}$. This equation is nothing but the Poisson equation for the electrostatic potential φ with ion and electron densities expressed in terms of φ. We remember the derivation in Section 4.1 as a preparation for generalization. We also introduce the Sagdeev potential, whose derivative is the right-hand-side of the equation (1.12). The usage of the Sagdeev potential helps us to analyze the Bohm equation.

Bohm analyzed the equation and showed that the condition $\mathcal{M} \geq 1$ ($u_0 \geq \sqrt{T_\mathrm{e}/m}$) must be satisfied to produce a monotony-decreasing electric potential. This condition is called *Bohm's criterion*. In actual plasma systems, a region before the entrance of the sheath, in which ions are accelerated by electric fields to satisfy Bohm's criterion, is considered to be self-organized. Such region is called *presheath*. We note that the formations of sheath and presheath are observed in particle simulations [71, 72].

Generalization of Bohm's criterion to include physical effects such as thermal effects and plasma species has been studied, same as the KdV and KP equations. For example, including the effect of ion temperature, this condition is modified as $u_0 \geq \sqrt{(T_\mathrm{e} + \gamma T_\mathrm{i})/m}$ corresponding to the modification of the ion sound speed (γ is the ion heat ratio). See Refs. [5, 23, 62] for reviews of the sheath and Bohm's criterion.

Bohm [8] also explained the relationship between Bohm's criterion and the creation of the sheath (see also Ref. [12]). Bohm's criterion corresponds to $\partial(n_\mathrm{i} - n_\mathrm{e})/\partial\varphi \leq 0$, where n_i and n_e are the ion and electron densities. When the electrostatic potential φ drops, both of the ion and electron densities decreases since ions gain speed and electrons are reflected. Bohm's criterion indicates that the decrease

rate of the electron density is larger than that of the ion density. The excess negative charge promotes the drop of the electrostatic potential, and the sheath is formed. We note that mathematical proofs of the relationship between Bohm's criterion and the stability condition of electrostatic potentials are also studied (see Ref. [54] and references therein).

1.6 Thermal effect and self-organization in plasma

The sheaths arise where plasmas hit walls—such as divertors of tokamaks. In such regions, we cannot ignore the effect of a heat flux coming from hot plasmas. Few studies consider the problems of coexistence of sheath and heat flux. Some studies on the scrape-off layer (SOL) region, which indicates the outside of the separatrix in a tokamak, emphasis thermal effects. However, they do not solve the inside of the sheath region but use boundary conditions at the sheath entrance, such as Bohm's criterion, obtained from sheath theories [68] or particle simulations [71, 72]. Some other works consider whole of the SOL region (e.g., Refs. [76, 77]), but they do not consider electrostatic fields.

Recently, Yoshida and Mahajan [87] considered a thermodynamical model of plasma boundary layers. They abstracted thermodynamical effects of self-organized structures in plasmas, such as zonal flow, and expressed as a parallel connected impedance. A parallel connected impedance means that the structure blocks heat fluxes. They showed that the bifurcation from a small temperature contrast to a larger one occurs when the heat flux entering the system exceeds a threshold. Kawazura and Yoshida [35, 36] extended the above work and found that the bifurcation feature, change of the temperature contrast, is reversed depending on the thermodynamical properties of self-organized plasma (blocking or promoting heat transport) and the controlled parameter (flux or temperature). Their works are abstract ones and thus valid for general systems. However, they assumed thermodynamical properties of plasmas and did not solve the equation of motion for plasmas.

To consider actual mechanisms of plasmas, we should solve the equations of plasma dynamics.

These surroundings motivate us to consider a problem in which the heat transport and the sheath coexists. That is the second objective of the dissertation.

1.7 Plan of dissertation

We have reviewed works on nonlinear ion acoustic waves—soliton and sheath. Most soliton equations obtained by reductive perturbation methods are vortex-free, and Yoshida formulated a minimal generalized system with finite vorticity. In Chapter 2, we show a proof of the fact that reductive perturbation method for the KP equation eliminates vorticity. We also give a detailed explanation for the derivation of the KPY equations. Subsequently, Chapter 3 is devoted to analyzing the integrability of the KPY equation. The Painlevé analysis shows that the equation is *not* integrable due to the three-dimensionality caused by the vortex field. Then we elucidate how a transition from soliton to chaos occurs by numerical simulation. These chapters are based on the published article [57] but contain some explanations, remarks, and numerical results are added. In Chapter 4, we solve a problem of thermal effects on the sheath. First, we assume the adiabatic ion temperature and obtain a set of two Bohm equations (Sagdeev potentials). The singularity of those potentials enables us to construct bifurcated solutions. Next, we include a heat diffusion which makes the usage of Sagdeev potentials impossible. We will see that both of the controlled parameter (heat flux or temperature) and the ion Mach number change the thermodynamical property (amounts of temperature contrast or heat flux). Finally, we summarize the obtained results in Chapter 5.

Chapter 2

Reductive Perturbation Methods and Vortex

In this chapter, we investigate the relation between reductive perturbation method and vortex.

Washimi and Taniuti [81] derived the KdV equation

$$\frac{\partial u}{\partial t} + \alpha u \frac{\partial u}{\partial x} + \beta \frac{\partial^3 u}{\partial x^3} = 0, \tag{2.1}$$

and Kako and Rowlands [32] derived the two-dimensional KP equation

$$\frac{\partial}{\partial x}\left(\frac{\partial u}{\partial t} + \alpha \frac{\partial u}{\partial x} + \beta \frac{\partial^3 u}{\partial x^3}\right) + \gamma \frac{\partial^2 u}{\partial y^2} = 0. \tag{2.2}$$

(In Section 2.1.1 we remember the derivation of the KdV and KP equations.) As referred in Section 1.1, various directions of generalizations have been studied. Most of them are directed to include many physical effects, such as thermal effects, multi-species, and higher-order effects.

However, these models do not have vorticities, and there have been few studies regarding this point, as far as we know. The KdV-type equation is a one-dimensional flat system, and thus it does not have enough freedom to have a vorticity. The KP-type equation also does not have a vorticity, although it is a multi-dimensional system. See Appendix A.3 for a significant role of vorticity in the hierarchy of fluid flows.

In Section 2.1, we show that the KP equation is derived by eliminating vorticity

at every order of the reductive perturbation. We also show that the reductive perturbation succeeds only if the entropy is homogeneous; hence the baroclinic effect, a creation mechanism of vorticity, must be absent. In Section 2.2, we follow the new ordering of velocity field proposed by Yoshida and derive a finite-vorticity system, the KPY equations. The new system is composed of a generalized three-dimensional KP equation and a two-dimensional vorticity equation. The former describes "scattering" of vortex-free waves by ambient vortexes that are determined by the latter. We say that the vortexes are "ambient" because they do not receive reciprocal reactions from the waves. Finally, we add some remarks about the new model in Section 2.3.

2.1 Reductive perturbation method for Kadomtsev–Petviashvili equation and vorticity

2.1.1 Korteweg–de Vries equation and Kadomtsev–Petviashvili equation

We start by remembering the derivation of the KdV and KP equations by the reductive perturbation method. The basic equations for nonlinear ion acoustic waves [12] are expressed as

$$\frac{\partial n}{\partial t} + \nabla \cdot (n\boldsymbol{u}) = 0, \tag{2.3}$$

$$\frac{\partial \boldsymbol{u}}{\partial t} + (\boldsymbol{u} \cdot \nabla)\boldsymbol{u} = -\nabla\varphi, \tag{2.4}$$

$$-\Delta\varphi = n - \mathrm{e}^{\varphi}, \tag{2.5}$$

where n is the ion number density, $\boldsymbol{u} = (u, v, w)^{\top}$ is the ion velocity, φ is the electrostatic potential, and $\Delta = \partial^2/\partial x^2 + \partial^2/\partial y^2 + \partial^2/\partial z^2$ is the Laplacian. We consider cold ions (except Section 2.1.4) and adiabatic electrons with a constant temperature T_e. We normalize the variables as followings: the density n by a representative density n_0, the velocity $\boldsymbol{u}$ by the ion sound speed $c_\mathrm{s} = \sqrt{T_\mathrm{e}/m}$ (where m is the ion mass), the electrostatic potential φ by the characteristic potential T_e/e, the coordi-

nate variable $\boldsymbol{x}$ by the Debye length $\lambda_{\mathrm{D}} = \sqrt{\varepsilon_0 T_{\mathrm{e}}/n_0 e^2}$, and the time variable t by the ion plasma frequency $\omega_{\mathrm{pi}} = \sqrt{n_0 e^2/\varepsilon_0 m}$.

Firstly, we derive the KdV equation. We consider ion acoustic waves propagating in the one-dimensional space (x). We introduce a set of stretched variables

$$\tilde{x} = \epsilon(x - t), \qquad \tilde{t} = \epsilon^3 t, \tag{2.6}$$

with a small parameter ϵ, and expand the dependent variables n, φ, and u as

$$\begin{cases} n = 1 + \epsilon^2 n_1 + \epsilon^4 n_2 + \cdots, \\ u = 0 + \epsilon^2 u_1 + \epsilon^4 u_2 + \cdots, \\ \varphi = 0 + \epsilon^2 \varphi_1 + \epsilon^4 \varphi_2 + \cdots. \end{cases} \tag{2.7}$$

Now we substitute the expansion to the equations (2.3)–(2.5) and evaluate each order terms. From the terms of orders ϵ^2 and ϵ^3, we obtain $n_1 = \varphi_1$ and $\partial n_1/\partial\tilde{x} = \partial u_1/\partial\tilde{x} = \partial\varphi_1/\partial\tilde{x}$. Assuming the boundary conditions $n_1, \varphi_1, u_1 \to 0$ $(x \to \pm\infty)$, we put

$$n_1 = u_1 = \varphi_1. \tag{2.8}$$

From the terms of order ϵ^4, we obtain

$$n_2 = \varphi_2 + \frac{\varphi_1^2}{2} - \frac{\partial^2\varphi_1}{\partial\tilde{x}^2}. \tag{2.9}$$

Then, from the terms of order ϵ^5 we obtain the KdV equation:

$$\frac{\partial u_1}{\partial\tilde{t}} + u_1\frac{\partial u_1}{\partial\tilde{x}} + \frac{1}{2}\frac{\partial^3 u_1}{\partial\tilde{x}^3} = 0. \tag{2.10}$$

Next, we drive the KP equation by considering ion acoustic waves propagating in the three-dimensional space (x, y, z). We assume that waves primarily propagate in the direction of x, and introduce stretched variables as

$$\tilde{y} = \epsilon^2 y, \qquad \tilde{z} = \epsilon^2 z, \tag{2.11}$$

in addition to the equation (2.6). The expansion of n, φ, and u are same as the equation (2.7), and we expand v and w as

$$\begin{cases} v = 0 + \epsilon^3 v_1 + \epsilon^5 v_2 + \cdots, \\ w = 0 + \epsilon^3 w_1 + \epsilon^5 w_2 + \cdots. \end{cases} \tag{2.12}$$

From the terms of orders ϵ^2 and ϵ^3, we obtain $n_1 = u_1 = \varphi_1$ same as the equation (2.8). From the terms of order ϵ^4, we obtain

$$\frac{\partial v_1}{\partial \tilde{x}} = \frac{\partial \varphi_1}{\partial \tilde{y}}, \tag{2.13}$$

$$\frac{\partial w_1}{\partial \tilde{x}} = \frac{\partial \varphi_1}{\partial \tilde{z}}, \tag{2.14}$$

and the equation (2.9). From the terms of order ϵ^5, we obtain the three-dimensional KP equation:

$$\frac{\partial}{\partial \tilde{x}} \left(\frac{\partial u_1}{\partial \tilde{t}} + u_1 \frac{\partial u_1}{\partial \tilde{x}} + \frac{1}{2} \frac{\partial^3 u_1}{\partial \tilde{x}^3} \right) + \frac{1}{2} \Delta_\perp u_1 = 0, \tag{2.15}$$

where $\Delta_\perp = \partial^2/\partial \tilde{y}^2 + \partial^2/\partial \tilde{z}^2$ is the Laplacian operator perpendicular to the primal propagating direction (x). Ignoring the velocity w and the z-dependence, the equation (2.15) reduces to the two-dimensional KP equation

$$\frac{\partial}{\partial \tilde{x}} \left(\frac{\partial u_1}{\partial \tilde{t}} + u_1 \frac{\partial u_1}{\partial \tilde{x}} + \frac{1}{2} \frac{\partial^3 u_1}{\partial \tilde{x}^3} \right) + \frac{1}{2} \frac{\partial^2 u_1}{\partial \tilde{y}^2} = 0. \tag{2.16}$$

2.1.2 Vorticity of Kadomtsev–Petviashvili equation

Strikingly absent in the KP equation is the vorticity. The expansion of the z-component of the vorticity $\omega_z = \partial v/\partial x - \partial u/\partial y$ is

$$\omega_z = \epsilon^4 \left(\frac{\partial v_1}{\partial \tilde{x}} - \frac{\partial u_1}{\partial \tilde{y}} \right) + \epsilon^6 \left(\frac{\partial v_2}{\partial \tilde{x}} - \frac{\partial u_2}{\partial \tilde{y}} \right) + \cdots. \tag{2.17}$$

The leading-order term turns out to be zero from equations (2.8) and (2.13). The same ordering applies to the y-component of the vorticity $\omega_y = \partial u/\partial z - \partial w/\partial x$; hence the leading-order vorticity vanishes by the demand of equations (2.8) and (2.14). The expansion of the x-component of the vorticity $\omega_x = \partial w/\partial y - \partial v/\partial z$ is

$$\omega_x = \epsilon^5 \left(\frac{\partial w_1}{\partial \tilde{y}} - \frac{\partial v_1}{\partial \tilde{z}} \right) + \epsilon^7 \left(\frac{\partial w_2}{\partial \tilde{y}} - \frac{\partial v_2}{\partial \tilde{z}} \right) + \cdots. \tag{2.18}$$

The ordering is slightly different from those of ω_y and ω_z. However, x-derivative of the leading-order term is forced to vanish by equations (2.8), (2.13), (2.14), and the boundary condition $\partial w_1/\partial\tilde{y} - \partial v_1/\partial\tilde{z} \to 0$ $(x \to \pm\infty)$. Thus, the KP system is vortex-free.

2.1.3 Vorticity of general order

The absence of vorticity is not only on the order of the KP equation but also on all orders of perturbations. Let us examine higher order equations. The second-order equation is linear with respect to the second-order variables and includes an inhomogeneous term depending on u_1 [27, 40, 75]. The higher order perturbations are called clouds surrounding the core, i.e., the first-order perturbation; a soliton with clouds is referred to as a dressed soliton. As proved in the previous section, *the core is vortex-free.* Moreover, we find that *all of the clouds are vortex-free.*

We obtain the vorticity equation by taking the curl $\nabla\times$ of the equation of motion (2.4):

$$\frac{\partial\boldsymbol{\omega}}{\partial t} = \nabla\times(\boldsymbol{u}\times\boldsymbol{\omega}). \tag{2.19}$$

There are no source terms since we consider only the potential force $-\nabla\varphi$. After the Galilean boost in the x-direction (see the equation (2.6)), the equation (2.19) reads as

$$\frac{\partial\boldsymbol{\omega}}{\partial t} - \frac{\partial\boldsymbol{\omega}}{\partial x} = \nabla\times(\boldsymbol{u}\times\boldsymbol{\omega}). \tag{2.20}$$

Inserting the expressions (2.6) and (2.7), and using equations (2.11), (2.12), (2.17), and (2.18), let us see the orders of each term in equation (2.20); in the x-component

$$\frac{\partial\omega_x}{\partial t} - \frac{\partial\omega_x}{\partial x} = \frac{\partial}{\partial y}(u\omega_y - v\omega_x) - \frac{\partial}{\partial z}(w\omega_x - u\omega_z), \tag{2.21}$$

the order of the second term on the left-hand-side is ϵ^6, while all other terms are of order ϵ^8. Thus, the lowest order vorticity ω_{x1} must satisfy

$$\frac{\partial\omega_{x1}}{\partial x} = 0. \tag{2.22}$$

Assuming the boundary condition $\omega_{x1} \to 0$ ($x \to \pm\infty$), we obtain $\omega_{x1} = 0$. In the y- and z-components of the equation (2.20) the orders of all terms decrease by ϵ^1; hence we obtain $\omega_{y1} = \omega_{z1} = 0$ under the boundary conditions $\omega_{y1}, \omega_{z1} \to 0$ ($x \to \pm\infty$).

Eliminating $\boldsymbol{\omega}_1$, the equation (2.20) reads as the equation for the second-order part of $\boldsymbol{\omega}$ ($\boldsymbol{\omega}_2$). By the same argument of ordering, we obtain $\boldsymbol{\omega}_2 = 0$, and the equation (2.20) dominates the next order. Continuing the induction, we conclude that $\boldsymbol{\omega}_j = 0$ for all order j.

2.1.4 Finite ion temperature effect

In the vorticity equation (2.20), the boost term $\partial\boldsymbol{\omega}/\partial x$ causes unbalance of ordering and forces the vorticity to vanish, when we invoke the standard expansion, equations (2.7) and (2.12). This ordering is tailor-made to match $n(\nabla \cdot \boldsymbol{v})$ and $\nabla\varphi$ with the boost terms in the continuity equation and the equation of motion.

In this section, we examine the effect of finite ion temperature T_i. It introduces a non-potential force $-n^{-1}\nabla p$ to the equation of motion (2.4) and a source term $\nabla T_\mathrm{i} \times \nabla s$ to the vorticity equation (2.19), where p is the ion pressure and s is the ion entropy. This production mechanism of vorticity is called the *baroclinic effect* [18, 60]. We show that the baroclinic effect must be absent for the success of the reductive perturbation method.

We apply the reductive perturbation method for the KP equation (Section 2.1.1). We assume that the ion pressure obeys the adiabatic equation

$$\frac{\partial p}{\partial t} + \boldsymbol{u} \cdot \nabla p + \gamma p(\nabla \cdot \boldsymbol{u}) = 0, \tag{2.23}$$

where γ is the ion heat ratio. We normalize the ion pressure by the representative pressure $n_0 T_\mathrm{e}$. We expand p as $p = \sigma + \epsilon^2 p_1 + \epsilon^4 p_2 + \cdots$, where $\sigma = T_{\mathrm{i}0}/T_\mathrm{e}$ is the normalized representative temperature. It should be noted that the speed of Galilean boost must be modified from 1 to $\lambda = \sqrt{1 + \gamma\sigma}$ (normalized with $c_\mathrm{s} = \sqrt{T_\mathrm{e}/m}$) [70]. This modification is due to the change of ion sound speed. The relations (2.8),

(2.13), and (2.14) are modified as

$$\begin{cases} \lambda n_1 = \lambda\varphi_1 = u_1 = \dfrac{\varphi_1 + p_1}{\lambda}, \\ \dfrac{\partial v_1}{\partial \tilde{x}} = \dfrac{1}{\lambda}\dfrac{\partial}{\partial \tilde{y}}(\varphi_1 + p_1), \\ \dfrac{\partial w_1}{\partial \tilde{x}} = \dfrac{1}{\lambda}\dfrac{\partial}{\partial \tilde{z}}(\varphi_1 + p_1), \end{cases} \tag{2.24}$$

and we obtain the KP equation

$$\frac{\partial}{\partial \tilde{x}}\left[\frac{\partial u_1}{\partial \tilde{t}} + \left(1 + \frac{\gamma+1}{2}\gamma\sigma\right) u_1 \frac{\partial u_1}{\partial \tilde{x}} + \frac{1}{2\lambda}\frac{\partial^3 u_1}{\partial \tilde{x}^3}\right] + \frac{\lambda}{2}\Delta_\perp u_1 = 0, \tag{2.25}$$

which reduces to equation (2.15) in the limit $T_\mathrm{i} = 0$ ($\sigma = 0$, $\lambda = 1$).

From the equation (2.24), we find that the lowest order vorticity is zero: $\omega_{x1} = \omega_{y1} = \omega_{z1} = 0$, same as the case of cold ions ($T_\mathrm{i} = 0$). Furthermore, we show that entropy must be homogeneous and thus baroclinic term must vanish for the success of the reductive perturbation method. We use the same procedure of Section 2.1.3. Let us consider the adiabatic evolution equation for entropy

$$\frac{\partial s}{\partial t} + \boldsymbol{u}\cdot\nabla s = 0, \tag{2.26}$$

which is equivalent to the pressure equation (2.23). The Galilean boost in the x-direction modifies the equation (2.26) as

$$\frac{\partial s}{\partial t} - \lambda\frac{\partial s}{\partial x} + \boldsymbol{u}\cdot\nabla s = 0. \tag{2.27}$$

Now we evaluate the orders of operators $\partial/\partial t$, $\lambda\partial/\partial x$, and $\boldsymbol{u}\cdot\nabla = u\partial/\partial x + v\partial/\partial y + w\partial/\partial z$ with equations (2.6), (2.7), (2.11), and (2.12). The order of the second operator is ϵ^1, and the lowest order of others is ϵ^3. Thus, the leading order term of the entropy s_0 must satisfy $\partial s_0/\partial x = 0$. This results in $s_0 = c$ (constant) under the boundary condition $s_0 \to c$ ($x \to \pm\infty$), which is a natural choice because s_0 is not a perturbation part. Eliminating s_0, equation (2.27) reads as the equation for s_1. The same discussion requires s_1 to satisfy $\partial s_1/\partial x = 0$. Since s_1 is a perturbation part, it is natural to use the boundary condition $s_1 \to 0$ ($x \to \infty$). These relations lead

to $s_1 = 0$. Repeating this procedure, we find that entropy must be homogeneous: $s = s_0 = c$. Thus, the baroclinic effect must vanish under the reductive perturbation method. (We do not consider the ion temperature effect in the rest of this chapter and the next chapter except in one of the comments on the end of this chapter.)

2.2 Generalized system with finite vorticity

In this section, we give a detailed explanation for the derivation of the KPY equations, a minimal generalization of KP equation with finite vorticity. The keys of the derivation are: (i) a certain order vorticity appears only in higher order dynamical equations; (ii) the vanishment of vorticities depends on the boundary condition $\boldsymbol{\omega} \to \mathbf{0}$ ($x \to \pm\infty$). We begin by explaining these points. (i) We may rewrite the equation of motion (2.4) in the following form:

$$\frac{\partial \boldsymbol{u}}{\partial t} - \boldsymbol{u} \times \boldsymbol{\omega} = \nabla \left(\varphi - \frac{1}{2} |\boldsymbol{u}|^2 \right). \tag{2.28}$$

Let us consider the x-component. The order of n-th perturbation velocity u_n is ϵ^{2n}, and those of corresponding vorticities ω_{yn} and ω_{zn} are ϵ^{2n+2} (see equation (2.17)). Hence the order of $\partial u_n/\partial t$ is ϵ^{2n+3}, and the lowest order of the second term with ω_{yn} and ω_{zn} $v_1\omega_{zn} - w_1\omega_{yn}$ is ϵ^{2n+5}. One finds that ω_{yn} and ω_{zn} do not appear in the dynamics of u_n but in higher order dynamics. In the y- and z-components, each order increases by ϵ, and we obtain the same result. (ii) The boundary condition $\boldsymbol{\omega}_n \to \mathbf{0}$ ($x \to \pm\infty$; $n = 1, 2, \dots$) is natural because perturbation parts should vanish at infinity. However, as shown in Sections 2.1.2 and 2.1.3, the combination of this boundary condition and $\partial\omega_{jn}/\partial x = 0$ forbids the existences of vorticities.

The point (i) induces us to add a lower order velocity. Addition of a lower order (ϵ^0) velocity in the x-direction is equivalent to a Galilean boosting, and it is improper because the boosting speed must be 1 (normalized with c_s) to make the reductive perturbation consistent. Therefore we introduce a velocity $\boldsymbol{v}_0 = (0, v_0, w_0)^\top$ of order

ϵ in the y- and z-directions:

$$\begin{cases} v = \epsilon v_0 + \epsilon^3 v_1 + \epsilon^5 v_2 + \cdots, \\ w = \epsilon w_0 + \epsilon^3 w_1 + \epsilon^5 w_2 + \cdots. \end{cases} \tag{2.29}$$

Next, considering the point (ii), we assume that the additional velocity is homogeneous in the x-direction: $\partial \boldsymbol{v}_0/\partial x = \boldsymbol{0}$. Moreover, to maintain the relation (2.8), we assume that $\boldsymbol{v}_0$ is incompressible: $\nabla \cdot \boldsymbol{v}_0 = 0$. The two-dimensionality and the incompressibility lead us to write $\boldsymbol{v}_0$ in the Clebsch form [85]

$$\boldsymbol{v}_0 = \nabla_\perp \psi(\tilde{y}, \tilde{z}) \times \boldsymbol{e}_x, \tag{2.30}$$

where $\boldsymbol{e}_x = \nabla x$ is the unit vector in the x-direction, ψ is the stream function, and $\nabla_\perp = (0, \partial/\partial\tilde{y}, \partial/\partial\tilde{z})$.

From the lowest order terms, we obtain the well-known two-dimensional Euler vorticity equation

$$\frac{\partial}{\partial \tilde{t}} \Delta_\perp \psi + [\Delta\psi, \psi] = 0, \tag{2.31}$$

where $\Delta_\perp \psi$ denotes the vorticity and $[f, g] = \boldsymbol{e}_x \cdot (\nabla_\perp f \times \nabla_\perp g) = (\partial f/\partial\tilde{y})(\partial g/\partial\tilde{z}) - (\partial f/\partial\tilde{z})(\partial g/\partial\tilde{y})$ is the convective term. From the terms of order ϵ^5, we obtain a three-dimensional wave equation:

$$\frac{\partial}{\partial \tilde{x}} \left(\frac{\partial u_1}{\partial \tilde{t}} + u_1 \frac{\partial u_1}{\partial \tilde{x}} + \frac{1}{2} \frac{\partial^3 u_1}{\partial \tilde{x}^3} + [u_1, \psi] \right) + \frac{1}{2} \Delta_\perp u_1 = 0. \tag{2.32}$$

We refer to the system of equations (2.31)–(2.32) as the Kadomtsev–Petviashvili–Yoshida (KPY) equations and compare it with the KP equation. In what follows, the subscript $_1$ and the tilde $\tilde{}$ will be omitted for simplicity.

The vortex field ψ ($-\Delta_\perp \psi$ is the vorticity) affects the ion acoustic wave field u through equation (2.32) while it does not receive any reciprocal reaction from u (notice that the vortex equation (2.31) is independent of u). This is because the order of ψ is lower than that of u. We may treat ψ as an "ambient" field for u (see Figure 2.1).

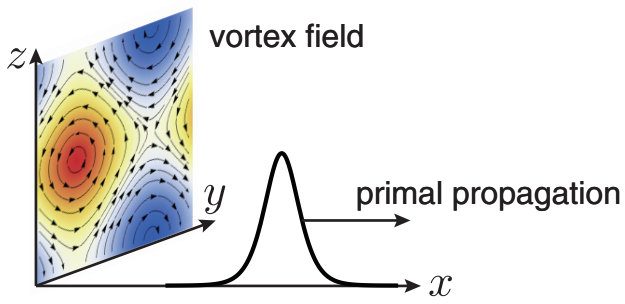

Figure 2.1: Conceptual diagram of the KPY equations (2.31)–(2.32). The solitary ion acoustic waves propagate in the ambient vortex field. The vortex field is perpendicular to the primal propagating direction of solitary waves.

In the next chapter, which is devoted to analyzing of the KPY equation, we assume that the vortex field ψ is stationary. For example, $\psi = a\sin(ky) - a\cos(kz)$ is a stationary solution of the Euler equation (2.31), which satisfies $\Delta_\perp \psi \propto \psi$. Then, only the equation (2.32), to be called the KPY equation, will be the objective of the analysis.

2.3 Additional remarks

The challenge of imparting vorticity to ion acoustic wave has been overcome by modifying the perturbative expansion of the velocity field. We close this chapter with some remarks.

(1) The KP equation (2.15) derived in Section 2.1 is the KP-II equation. (The equation with the sign of $\Delta_\perp u$ reversed is called the KP-I equation.) Although both of KP-I and KP-II equations are soliton equation, the shapes of soliton solution are completely different. The stable line soliton of the KP-II equation becomes unstable in the KP-I equation and changes its shape to other soliton solution, which is called the *lump soliton* [28, 29, 67].

(2) As we have shown in Section 2.1.3, the absence of vorticity is a strong imprint made by the ordering that characterizes the KP system. This constraint is ubiquitous

among the families including a finite-temperature model (see Section 2.1.4), trapped electron model, and multi-component models. It is because the former only increases the number of equations and the latter only changes the Poisson equation, they do not modify the structure of the equation of motion.

(3) We note that baroclinic effect vanishes even in the KPY equations. This is because the discussion of Section 2.1.4 is valid even if we introduce the additional velocity $\boldsymbol{v}_0$ as the equation (2.29). Finite ion temperature modifies the KPY equation (2.32) as

$$\frac{\partial}{\partial\tilde{x}}\left[\frac{\partial u_1}{\partial\tilde{t}}+\left(1+\frac{\gamma+1}{2}\gamma\sigma\right)u_1\frac{\partial u_1}{\partial\tilde{x}}+\frac{1}{2\lambda}\frac{\partial^3 u_1}{\partial\tilde{x}^3}+[u_1,\psi]\right]+\frac{\lambda}{2}\Delta_\perp u_1=0, \tag{2.33}$$

without changing the Euler vorticity equation (2.31).

(4) The new ordering of the velocity field enables us to study the neighborhood of the integrable KP hierarchy. At the lowest order, i.e., the KPY system, however, the range of dynamics is still rather narrow—the *helicity* $\int \boldsymbol{u}\cdot\boldsymbol{\omega}\,\mathrm{d}^3x$ is zero. We can prove this fact with the constraint

$$\int \Delta_\perp u\,\mathrm{d}x=0, \tag{2.34}$$

which is derived by integrating the KPY equation (2.32) in the x-direction and assuming the periodic boundary condition. We note that this constraint is also valid for the KP equation and requires careful attentions (see Ref. [38] and references therein). Since ψ is independent of x and $\Delta_\perp$ is a self-adjoint operator, we obtain

$$\int u\Delta_\perp\psi\,\mathrm{d}^3x=\int\psi\Delta_\perp u\,\mathrm{d}^3x=\int\psi\left(\int\Delta_\perp u\,\mathrm{d}x\right)\mathrm{d}y\,\mathrm{d}z=0. \tag{2.35}$$

Instead of the helicity, the generalized enstrophy $\int g(\Delta_\perp\psi)\,\mathrm{d}^2x$ has a finite value and is conserved (g is an arbitrary function). This constancy of the integral is due to the geometrical constraints that the velocity of KP equation is vortex-free ($\boldsymbol{u}_{\mathrm{KP}}$ can be expressed as $\nabla\chi$) and that of two-dimensional Euler equation is locally helicity-free ($\boldsymbol{u}_{\mathrm{Euler}}$ can be expressed as $\alpha\nabla\beta$). The summation of such two velocity

fields is called the *epi-two-dimensional flow* [88] (see also Appendix A.3.2). When one more velocity field $\alpha'\nabla\beta'$ is added to $\boldsymbol{u}_{\mathrm{KP}} + \boldsymbol{u}_{\mathrm{Euler}}$, the enstrophy is freed to increase, and the helicity has a finite value. This is the Clebsch representation of a three-dimensional flow [85] and describes a full development of turbulence.

Chapter 3

Non-Integrability of Ion Acoustic Waves Scattered by Vortexes

In the previous chapter, we prove that the reductive perturbation method used for deriving the KP equation eliminates vorticity, and derive the KPY equation (2.31)–(2.32) with finite vorticity. We may view the ordered system of solitons as a singular submanifold (leaf) embedded in a larger phase space of finite-vorticity perturbations [89]. The departure from the zero-vorticity leaf will produce complexity and, finally, generate turbulence. The aim of this generalization is to probe into the "neighborhood" of the KP hierarchy and elucidate how chaos starts to develop.

This chapter is devoted to investigating the integrability of the KPY equation (2.32) (as described in the last of Section 2.2, we assume that the vortex field ψ is stationary). We use Painlevé test, which is well-known as a useful method for evaluating the integrability, and numerical analysis.

In Section 3.1 we briefly review the Painlevé test for partial differential equation (PDE) proposed by Weiss, Tabor, and Carnevale (WTC) [83]. The original WTC method produces complicated calculation, and improved methods reducing calculations has been proposed. We introduce two methods: Kruskal's one [30, 83] and Conte's one [14]. In Section 3.2, we invoke the Painlevé test with the WTC–Conte method to study whether the KPY equation (2.32) is integrable or not. The result

is negative. By this analysis, we elucidate that the scattering by the vorticity introduces an essential three-dimensionality to the ion acoustic wave fields, by which the integrability condition (in the sense of the Painlevé test) is broken. In Section 3.3, we perform numerical simulations to visualize how chaos occurs, which cannot be predicted by the Painlevé test. In Section 3.4, we conclude our investigations.

3.1 Brief review of Painlevé analysis for partial differential equation

When a nonlinear ordinary differential equation (ODE) has no movable critical points, the ODE is said to have the *Painlevé property*. Singularities of linear ODEs do not move; for example, $\mathrm{d}u/\mathrm{d}x = -u/x^2$ has a solution $u = u_0\mathrm{e}^{1/x}$ (u_0 is the integral constant) whose singularity $x = 0$ is fixed. On the other hand, singularities of nonlinear ODEs may move; for example, $\mathrm{d}u/\mathrm{d}x = -u^2$ has a solution $u = 1/(x-x_0)$ (x_0 is the integral constant) whose singularity $x = x_0$ is movable. A singularity of nonlinear ODE which is expressed as $u \sim (z - z_0)^{-p}$ with a positive integer p is called the *pole*, and a singularity which is not a pole is called the *critical point*. The Painlevé property is considered to be equivalent to the integrability.

As an extension of the Painlevé analysis for PDEs, Ablowitz, Ramani, and Segur (ARS) [1, 2] proposed the conjecture that *every ODE derived from an integrable PDE by a reduction has the Painlevé property*. If this conjecture is true, it provides a necessary condition to verify whether a given PDE is integrable or not. However, it is rarely useful since we cannot check *all* of ODEs derived from a PDE, and ODEs obtained from a non-integrable PDE may have the Painlevé property.

Weiss, Tabor, and Carnevale (WTC) [83] proposed another procedure to verify the integrability of PDEs by simply extending the definition of the Painlevé property for ODE. Their definition is as following: a nonlinear PDE is said to have the Painlevé property when the solutions are represented in terms of a Laurent series in a neighborhood of a movable singularity manifold (to be identified as a set of points satisfying $\varphi(x, y, z, t) = 0$). The Painlevé property is tested by assuming that the

solution $u(x,y,z,t)$ of a PDE can be written, in the neighborhood of the singularity manifold, as

$$u(x,y,z,t) = \chi^{-q} \sum_{j=0}^{\infty} u_j(x,y,z,t)\chi^j \tag{3.1}$$

with analytic functions u_j and an expansion function χ which vanishes as $\varphi \to 0$, and verifying whether q is a positive integer and all u_j's can be determined consistently. This procedure is called the *Painlevé test*. If a given PDE passes the test, we may obtain some outgrowths such as Lax pair [82].

There are various choices of the expansion function χ. The simplest one is $\chi = \varphi$ used by WTC [83], but this choice makes u_j complicated. For example, as the result of the Painlevé test for the KdV equation $\partial_t u + u\partial_x u + \partial_x^3 u = 0$, we obtain $u_0 = -12(\varphi_x)^2$, $u_1 = 12\varphi_{xx}$, $u_2 = -[\varphi_x\varphi_t + 4\varphi_x\varphi_{xxx} - 3(\varphi_{xx})^2]/(\varphi_x)^2 = 0$, $u_3 = (\varphi_{xt} + \varphi_{xx}u_2 + \varphi_{xxxx})/(\varphi_x)^2$, and so on (subscripts denote derivatives, e.g., $\varphi_x = \partial\varphi/\partial x$). The complexity comes from the derivatives of the expansion function χ. Kruskal proposed the expression $\varphi(x,t) = x - f(t)$ [30, 83]. This choice significantly reduces calculation, e.g., for the KdV equation $\partial_t u + u\partial_x u + \partial_x^3 u = 0$ we obtain $u_0 = -12$, $u_1 = 0$, $u_2 = \psi'$, $u_3 = 0$, and so on. Some computer programs of Painlevé analysis with Kruskal's choice are developed (e.g. Ref. [84]). However, this choice loses outgrowths of the analysis such as Lax pair.

Conte [14] showed that the best choice for reducing the calculation without any constraints on φ is

$$\chi = \left(\frac{\varphi_x}{\varphi} - \frac{\varphi_{xx}}{2\varphi_x}\right)^{-1}. \tag{3.2}$$

(A constraint $\varphi_x = 0$ is required, but this is also necessary for WTC and other choices.) The reason why the choice reduces calculation is that the derivatives of the expansion function χ can be written as polynomials of χ:

$$\chi_x = 1 + \frac{S}{2}\chi^2, \qquad \chi_t = -A + A_x\chi - \frac{1}{2}(A_{xx} + AS)\chi^2 \tag{3.3}$$

with $A = -\varphi_t/\varphi_x$ and $S = \varphi_{xxx}/\varphi_x - (3/2)(\varphi_{xx}/\varphi_x)^2$. Applying this choice for the KdV equation $\partial_t u + u\partial_x u + \partial_x^3 u = 0$, we obtain $u_0 = -12$, $u_1 = 0$, $u_2 = A - 4S$,

$u_3 = -A_x + S_x$, and so on.

WTC's Painlevé property is considered to be equivalent to the integrability of a PDE, and indeed many integrable equations (e.g., the Burgers equation, the KdV equation, and the two-dimensional KP equation) pass the Painlevé test [83]. However, the three-dimensional KP equation does not pass the test [11, 63, 84], and it is not integrable (see, e.g., Ref. [48] for another explanation of its non-integrability). See, e.g., Refs. [15, 42, 52] for details of the Painlevé analysis.

3.2 Painlevé test of Kadomtsev–Petviashvili–Yoshida equation

Now we execute the Painlevé test for the KPY equation (2.32) and show that the KPY equation passes the Painlevé test only under some special conditions.

In order to elucidate when the equation is integrable or not, we use a generalized form

$$u_{xt} + (uu_x)_x + \alpha u_{4x} + \beta u_{yy} + \gamma u_{zz} + a(y,z)u_{xy} + b(y,z)u_{xz} = 0, \tag{3.4}$$

where subscripts denote derivatives, α, β, γ are constants with $\alpha \neq 0$, and a, b are functions of y, z. In the original form (2.32), coefficients are chosen as $\alpha = 1$, $\beta = \gamma = 1/2$, $a(y,z) = \partial\psi/\partial z$, and $b(y,z) = -\partial\psi/\partial y$.

We apply Conte's choice (3.2) in the test. Since the system is three-dimensional, in addition to the equations (3.3) for χ_x and χ_t, we use the expressions for χ_y and χ_z:

$$\chi_y = -B + B_x\chi - \frac{1}{2}(B_{xx} + BS)\chi^2, \qquad \chi_z = -C + C_x\chi - \frac{1}{2}(C_{xx} + CS)\chi^2 \tag{3.5}$$

with $B = -\varphi_y/\varphi_x$ and $C = -\varphi_z/\varphi_x$. We also use relations for the derivatives of S:

$$S_t + A_{xxx} + 2A_xS + AS_x = 0, \tag{3.6}$$

$$S_y + B_{xxx} + 2B_xS + BS_x = 0, \tag{3.7}$$

$$S_z + C_{xxx} + 2C_xS + CS_x = 0. \tag{3.8}$$

The leading-order analysis (substituting $u = u_0\chi^{-q}$ and comparing leading-order terms) determines the values of q and u_0 as $q = 2$ and $u_0 = -12\alpha$. From general order terms, we obtain recursion relations

$$(j+1)(j-4)(j-5)(j-6)\alpha u_j = F_j(u_0, \ldots, u_{j-1}) \tag{3.9}$$

for $j = 1, 2, \ldots$, where F_j's are complicated functions of $u_0, \ldots, u_{j-1}$, φ, and their derivatives. u_1, u_2, and u_3 are determined by the equation (3.9) as

$$u_1 = 0, \tag{3.10}$$

$$u_2 = A - 4\alpha S - \beta B^2 - \gamma C^2 + aB + bC, \tag{3.11}$$

$$u_3 = -A_x + \alpha S_x + \beta(BB_x - B_y) + \gamma(CC_x - C_z) - aB_x - bC_x \tag{3.12}$$

If $F_4 = F_5 = F_6 = 0$ (called the *resonance condition*) is satisfied without putting constraints on φ, we can determine all u_j's consistently with arbitrary functions u_4, u_5, and u_6. However, we find $F_4 = F_5 = 0$ but $F_6 \neq 0$—the KPY equation does not pass the test and is not integrable. The expression for F_6 is as following:

$$F_6 = \beta\gamma E_1(\varphi) + \beta E_2(a_y, a_{yy}, b_y, b_{yy}; \varphi) + \gamma E_3(a_z, a_{zz}, b_z, b_{zz}; \varphi), \tag{3.13}$$

$$E_1 = \frac{4}{\varphi_x^4}[\varphi_x^2(\varphi_{yy}\varphi_{yz} - \varphi_{yz}^2) + 2\varphi_x\varphi_y(\varphi_{xz}\varphi_{yz} - \varphi_{xy}\varphi_{zz}) + \circlearrowleft_{x,y,z}], \tag{3.14}$$

$$\begin{aligned} E_2 = \frac{1}{\varphi_x^3}[&-a_{yy}\varphi_x^2\varphi_y - b_{yy}\varphi_x^2\varphi_z - 2a_y\varphi_x^2\varphi_{yy} - 2b_y\varphi_x^2\varphi_{yz} \\ &+ 2(2a_y + b_y)\varphi_x\varphi_z\varphi_{xy} + 2b_y\varphi_x\varphi_y\varphi_{xz} - 2b_y\varphi_{xx}\varphi_y\varphi_z - 2a_y\varphi_{xx}\varphi_y^2], \end{aligned} \tag{3.15}$$

$$\begin{aligned} E_3 = \frac{1}{\varphi_x^3}[&-a_{zz}\varphi_x^2\varphi_y - b_{zz}\varphi_x^2\varphi_z - 2a_z\varphi_x^2\varphi_{yz} - 2b_z\varphi_x^2\varphi_{zz} \\ &+ 2(a_z + 2b_z)\varphi_x\varphi_y\varphi_{xz} + 2a_z\varphi_x\varphi_z\varphi_{xy} - 2a_z\varphi_{xx}\varphi_y\varphi_z - 2b_z\varphi_{xx}\varphi_z^2], \end{aligned} \tag{3.16}$$

where $\circlearrowleft_{x,y,z}$ denotes the summation over cyclic permutation of x, y, z.

Since the additional vortex field is perpendicular to the primal direction of propagation, it brings about an essential three-dimensionality. Thus, it is expected that the KPY equation (2.32) is not integrable. The resonance condition $F_6 = 0$ is satisfied only in the following special cases: (i) $\beta = \gamma = 0$; (ii) $\gamma = 0$, $a_y = b_y = 0$;

(iii) $\beta = 0$, $a_z = b_z = 0$. In the case (i), the KPY equation (3.4) is reduced to the one-dimensional (x) KdV equation with convection terms in the independent directions (y, z). In the case (ii), the KPY equation is reduced to the two-dimensional (x, y) KP equation with boosting in the z-direction (whose speed is homogeneous in x- and y-directions). The case (iii) is same as the case (ii), with y and z exchanged. The cases (ii) and (iii) are consistent with integrable conditions (1.7) of generalized variable-coefficient two-dimensional KP equations (1.6) [74].

From the above result, we find that the KPY equation is integrable only if it can be reduced to a lower dimensional integrable system (the one-dimensional KdV equation or the two-dimensional KP equation). Therefore, the transition from soliton (of the two-dimensional KP equation) to chaos is expected to occur. In the next section, we demonstrate chaotic behaviors of ion acoustic wave by numerical solutions of the KPY equation.

3.3 Numerical analysis

3.3.1 Numerical scheme

We perform numerical simulation by the following setting. We consider a domain $(x, y, z) \in [0, 20] \times [-5, 5] \times [-5, 5]$ with the periodic boundary condition.

We split the KPY equation (2.32) as the following form:

$$\frac{\partial u}{\partial t} = \mathcal{L}u + \mathcal{N}(u), \tag{3.17}$$

$$\mathcal{L}u = -\frac{1}{2}\frac{\partial^3 u}{\partial x^3} - \frac{1}{2}\partial_x^{-1}\Delta_\perp u, \tag{3.18}$$

$$\mathcal{N}(u) = -\frac{1}{2}\frac{\partial}{\partial x}(u^2) - [u, \psi], \tag{3.19}$$

where ∂_x^{-1} is the inverse of differential operator $\partial/\partial x$ called the *anti-derivative*. The linear operator $\mathcal{L}$ contains the third-order differential operator $\partial^3 u/\partial x^3$ which restricts the time step to a small value in explicit schemes (Courant–Friedrichs–Lewy condition [61]). Here we solve the linear part implicitly with the Fourier transform.

On the other hand, we cannot easily approximate the nonlinear term with an implicit scheme. Here we use the second-order Strang splitting method [69]

$$u_{n+1} = \exp\left(\frac{h}{2}\mathcal{L}\right)\exp(h\mathcal{N})\exp\left(\frac{h}{2}\mathcal{L}\right)u_n, \tag{3.20}$$

where h is the time step size, and applying different schemes to $\mathcal{L}$ and $\mathcal{N}$. Each factor on the right-hand side of the equation (3.20) must be approximated by a second or higher order scheme. The linear part $\exp(h\mathcal{L})$ is solved implicitly with the Fourier transformation, and the nonlinear part $\exp(h\mathcal{N})$ is approximated by the second-order explicit Runge–Kutta method with finite-difference approximations. Since we use an exact solution of the two-dimensional Euler vortex equation for ψ, we may approximate the term $[u, \psi]$ with the ordinary central difference method.

A serious problem in the numerical calculation is the anti-derivative ∂_x^{-1} in the linear operator $\mathcal{L}$. We may evaluate this operator with a multiplier $1/(\mathrm{i}k_x)$ in the Fourier space.[1)] In order to regularize the singularity at $k_x = 0$, this multiplier is modified as $-\mathrm{i}/(k_x + \mathrm{i}\delta)$, with a small real number δ [22, 37, 38]. We use the machine epsilon of the double precision floating point number $2^{-52} \sim 2.2 \times 10^{-16}$, which is seen as almost zero in the numerical calculation. It should be noted that when the sign before $\partial_x^{-1}\Delta_\perp u$ is reversed, the sign of $+\mathrm{i}\delta$ must also be reversed. This reversal occurs not only in the KP-I equation but also applying higher-order splitting schemes [49] to the KP-II equation.

We note that there are some developments of numerical schemes for the KP equation, such as the window method for non-periodic boundary conditions [7, 34] and the characteristics method for the nonlinear term $u\partial_x u$ [22]. However, we cannot apply them for the KPY equation due to the term $[u, \psi]$.

We give an initial condition by modifying a line-soliton solution of the two-

[1)] When the boundary condition is not periodic, we cannot use Fourier transformation. In such situation, we must calculate the anti-derivative with direct integration. Assuming the domain of x-direction is $(-\infty, \infty)$, simple forms are $\partial_x^{-1}u = \int_{-\infty}^{x} u(x')\,\mathrm{d}x'$ or $\partial_x^{-1}u = -\int_{x}^{\infty} u(x')\,\mathrm{d}x'$. Another form is $\partial_x^{-1}u = \frac{1}{2}(\int_{-\infty}^{x} u(x')\,\mathrm{d}x' - \int_{x}^{\infty} u(x')\,\mathrm{d}x')$. The last form is an anti-symmetric operator and often used (see, e.g., Ref. [3]).

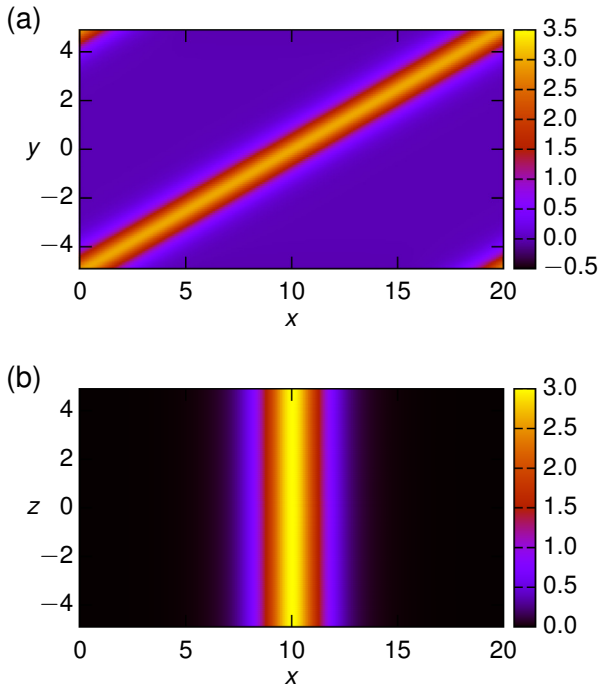

Figure 3.1: Cross-sections of u at $t = 0$ (a line-soliton with the periodic boundary condition, which is homogeneous in the z-direction). (a) $(z = 0)$-cross-section, (b) $(y = 0)$-cross-section.

dimensional KP equation:

$$u_0(x, y, z) = 3A \operatorname{sech}^2 \left[\sqrt{\frac{A}{2}} (x - By - C) \right], \tag{3.21}$$

where A, B, and C are arbitrary constants (we choose $A = 1$, $B = 2$, and $C = 10$). To put the waves in the periodic domain, x and y are, respectively, modulo 20 and 10 (box sizes). Furthermore, u must satisfy the constraint

$$\int \Delta_\perp u \, \mathrm{d}x = 0. \tag{3.22}$$

By subtracting the Fourier components with $k_x = 0$ (k_x is the wavenumber in the x direction), excepting the $k_x = k_y = k_z = 0$ component, from $u_0(x, y, z)$, we obtain the hoped-for initial condition (Figure 3.1). The KP equation (i.e., $\psi = 0$), starting from this initial condition, propagates with conserving the wave shape.

As described at the end of Section 2.2, we assume that ψ is stationary. We use

$$\psi(y,z) = a\sin\left(\frac{2\pi\kappa y}{L}\right) - a\cos\left(\frac{2\pi\kappa z}{L}\right), \tag{3.23}$$

where L is the length of the domain in the y- and z-directions ($L = 10$). a and κ denote the intensity and the wavenumber of the vortex field. κ must be an integer due to the periodic boundary condition.

3.3.2 Numerical results

When $a = 0$ (vortex-free), a line-soliton propagates without changing its shape. We change the value and observe how line-solitons are "scattered" by the vortex.

Figures 3.2 and 3.3 show y- and z-cross-sections of u with $a = 0.06$ and $\kappa = 2$. In Figure 3.2, we observe deformations in the y-cross-sections: (i) to the right side (Figure 3.2(a)); (ii) to both sides (Figure 3.2(b)); (iii) to the left side (Figure 3.2(c)); (iv) after (i)–(iii), u returns to the initial shape, homogeneous in the z-direction (Figure 3.2(d)). We find that the deformations (i)–(iv) are repeated periodically. In the z-cross-section, compared to the y-cross-section, noticeable deformations are not found (Figure 3.3). From these results, we can say that line-solitons (homogeneous in the z-direction) are "stable" against "weak" vortexes.

This stability is considered as due to the property of the KP-II equation. As described in Section 2.3, for the three-dimensional KP-I equation, it is known that perturbed line-solitons break up to lump solutions [28, 29, 67].

Figures 3.4 and 3.5 show y- and z-cross-sections of u with a larger value of a ($a = 0.30$). In the y-cross-section (Figure 3.4), we observe divided structures without returning to the initial shape. Furthermore, differently from the result of $a = 0.06$, deformations in the z-cross-section is also observed (Figure 3.5). When a is further large, u breaks up into small structures and spreads, as found in Figure 3.6. These results show scatterings of line-solitons due to the ambient vortex fields, and they can be regarded as effects of the non-integrability.

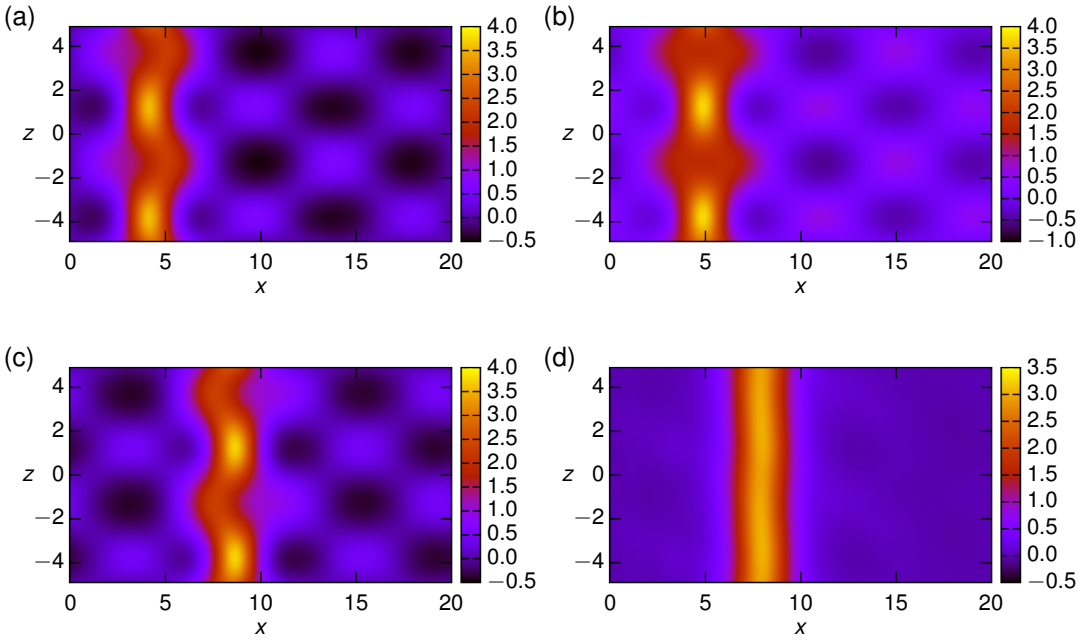

Figure 3.2: $(y = 0)$-cross-sections of u with $a = 0.06$ and $\kappa = 2$ at (a) $t = 25$, (b) $t = 32$, (c) $t = 40$, and (d) $t = 60$. (a)–(c): the direction of deformation is changed with time. (d): after the deformation, u becomes homogeneous in z-direction, as in the initial state (Figure 3.1(b)).

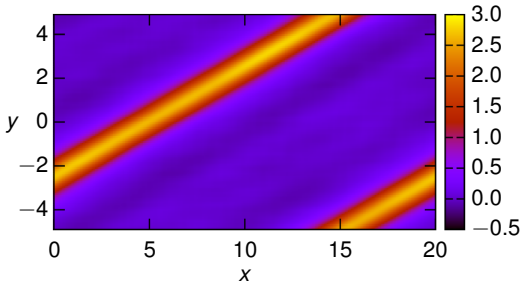

Figure 3.3: $(z = 0)$-cross-section of u with $a = 0.06$ and $\kappa = 2$ at $t = 32$. We do not find noticeable deformations compared to the y-cross-section (Figure 3.2)

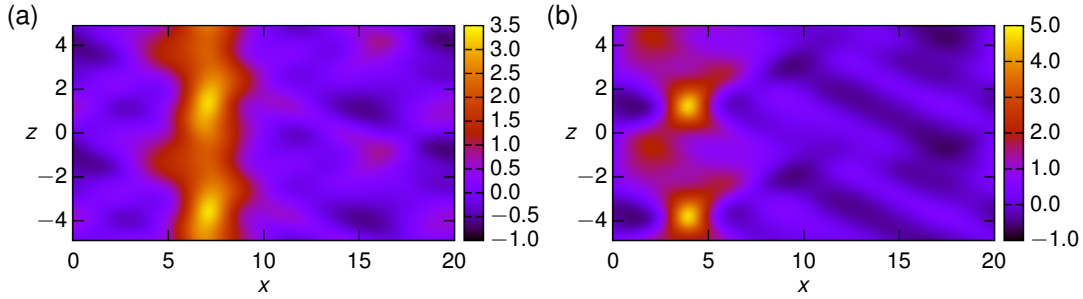

Figure 3.4: ($y = 0$)-cross-sections of u with $a = 0.30$ and $\kappa = 2$ at (a) $t = 20$ and (b) $t = 40$. A line structure is divided.

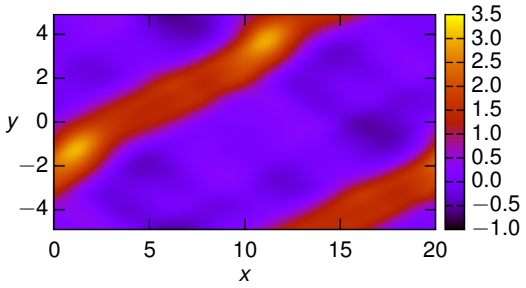

Figure 3.5: ($z = 0$)-cross-section of u with $a = 0.30$ and $\kappa = 2$ at $t = 40$. Compared to the case of $a = 0.06$ (Figure 3.2), z-cross section is clearly twisted.

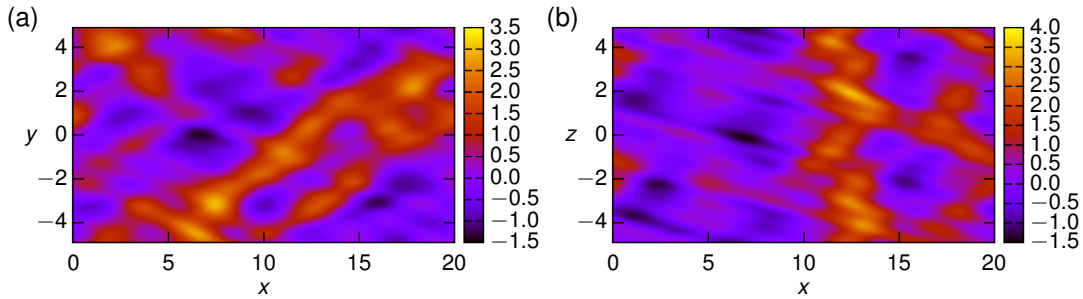

Figure 3.6: Cross-sections of u at $t = 40$ with $a = 1.0$ and $\kappa = 2$: (a) ($z = 0$)-cross-section, (b) ($y = 0$)-cross-section. The wave field breaks up into small structures and spreads into the whole of space.

In order to evaluate the above observations quantitatively, we calculate the average wavenumber

$$\langle k_j \rangle = \frac{\sum_{\boldsymbol{k}} k_j |\hat{u}_{\boldsymbol{k}}|^2}{\sum_{\boldsymbol{k}} |\hat{u}_{\boldsymbol{k}}|^2} \quad (j = x, y, z), \tag{3.24}$$

where $\hat{u}_{\boldsymbol{k}}$'s are Fourier coefficients of u. Figure 3.7 shows the evolution of the average wavenumber $\langle k_y \rangle$ with $a = 0.02$, 0.04, 0.06, and 0.08 ($\kappa = 2$ is fixed). We can find that the evolution looks like periodic and the period becomes short when a becomes large. Figure 3.8 shows the evolution of $\langle k_y \rangle$ with $a = 0.08$, 0.09, and 0.10. A transition from the periodic behavior ($a = 0.08$) to the increasing behavior ($a = 0.09, 0.10$) is found. As shown in Figure 3.9, the average wavenumber has a large value when a is further large. In this stage, periodic behaviors are not observed. We also find that the value of the average wavenumber is not clearly different between in the case of $a = 0.8$ and in that of $a = 1.0$. When κ has a large value, the average wavenumber is found to grow larger (Figure 3.10). Thus, we can say that scattering scales of line-solitons depend on the intensity and the spatial scales of the ambient vortex fields.

In the transition from soliton to chaos, we observe periodic behaviors. Additionally, we also find periodic behavior with two frequencies as Figure 3.11. We plot the frequencies of these calculations in Figure 3.12. The frequencies increase linearly with the amplitude a of the vortex field ψ. We should note that there are many high-frequency oscillation components and we pick out major part. The emergence of two frequencies indicates that the second major part grows.

We summarize the result of transitions from periodic behavior to growing behavior in Table 3.1. The values of amplitude a when the transitions occur are different with respect to the value of spatial scale of the vortex field κ.

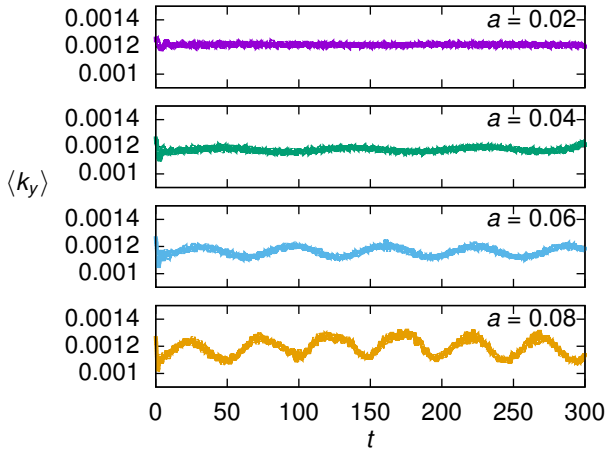

Figure 3.7: Evolution of average wavenumber $\langle k_y \rangle$ with $a = 0.02, 0.04, 0.06, 0.08$ ($\kappa = 2$). We observe periodic evolution and the period becomes shorter with the value of a increasing.

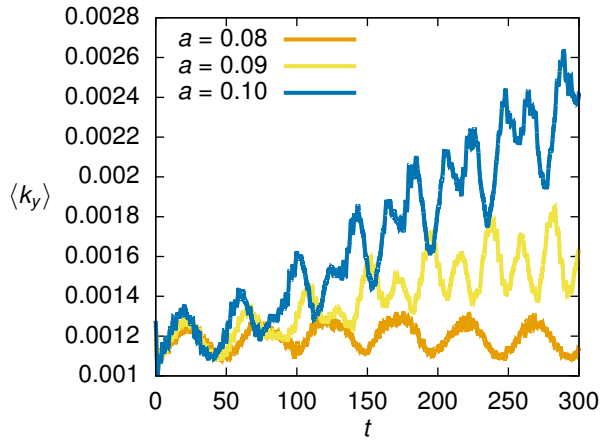

Figure 3.8: Evolution of average wavenumber $\langle k_y \rangle$ with $a = 0.08, 0.09, 0.10$ ($\kappa = 2$). The evolution transits from periodic one ($a = 0.08$) to growing ones ($a = 0.09, 0.10$).

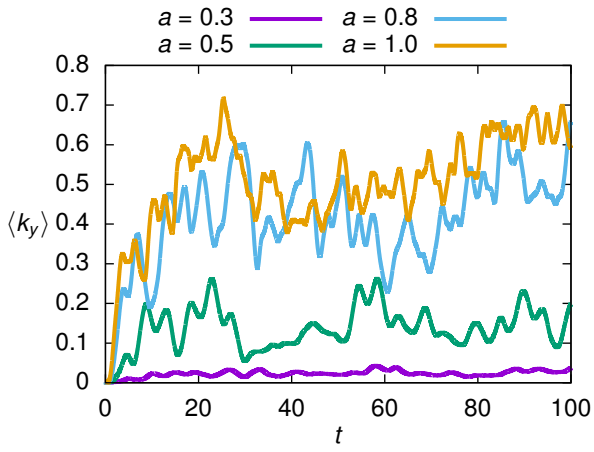

Figure 3.9: Evolution of average wavenumber $\langle k_y \rangle$ with $a = 0.3, 0.5, 0.8, 1.0$ ($\kappa = 2$). The average wavenumber has a large value when a is further large compared to Figure 3.8.

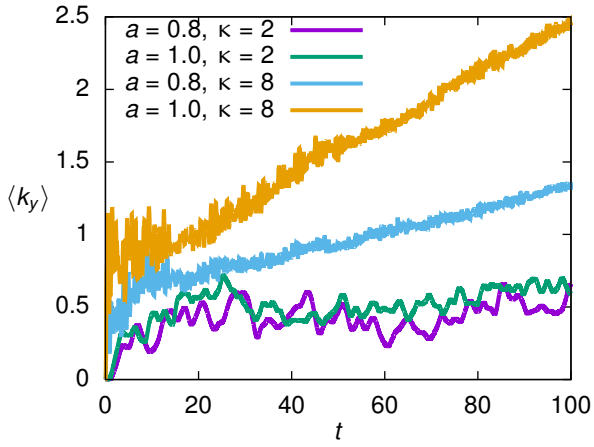

Figure 3.10: Evolution of average wavenumber $\langle k_y \rangle$ with $(a, \kappa) = (0.8, 2), (1.0, 2), (0.8, 8), (1.0, 8)$. Although the values of the average wavenumbers are rarely different between in the case of $a = 0.8$ and in that of $a = 1.0$ with $\kappa = 2$, they grow greater with a large κ.

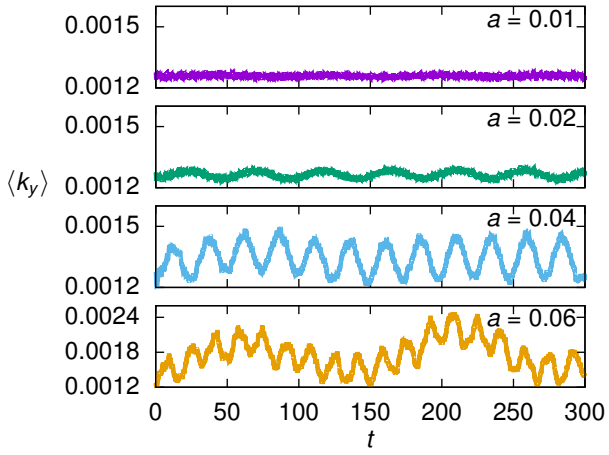

(a)

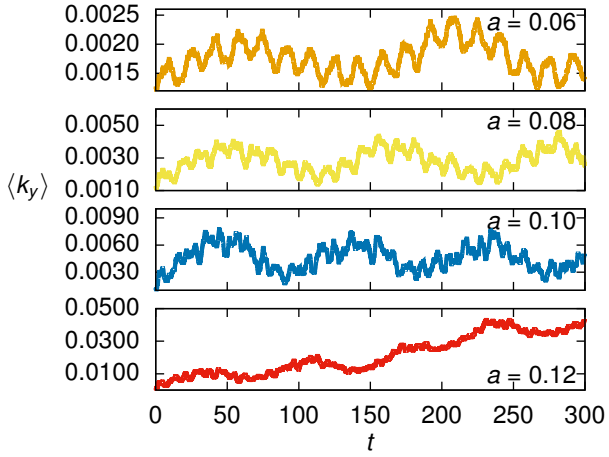

(b)

Figure 3.11: Multi-frequency behavior in the evolution of average wavenumbers. (a) From $a = 0.01$ to $a = 0.06$: we observe periodic behaviors in $a \leq 0.02$ and double-periodic behaviors in $a \geq 0.04$. (b) From $a = 0.06$ to $a = 0.12$: we observe double-periodic behavior in $a \leq 0.10$ and increase in $a = 0.12$.

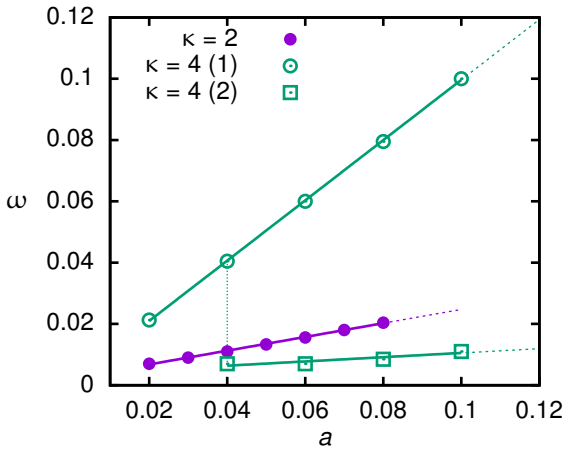

Figure 3.12: Relation between frequency ω of the averaged-wavenumber evolution and the amplitude of the vortex field a. The frequencies increase linearly with the amplitude.

Table 3.1: Transition in the evolution of average wavenumbers. "P" indicate the periodic evolution, "T" indicates the evolution with two frequencies, and "G" indicate that the wavenumber grows.

$\kappa \setminus a$	0.02	0.04	0.08	0.09	0.10	0.11
2	P	P	P	G	G	G
3	P	P	P	P	G	G
4	P	T	T	T	T	G
6	T	T	T	G	G	G

Now we study what happens in the transitions. First, we consider the transition from periodic behaviors to that of increasing wavenumbers. In order to see what occurs at the transition, we show the spectrum of $|u_{k_z}|^2$ in Figure 3.13. In the case of $a = 0.02$, the component $k_z = 2$ is greater then other components. When a becomes larger, the cases of $a = 0.06$ and $a = 0.08$, amplitudes of all components increase. However, higher wavenumber ($k_z \geq 4$) components increase more than $k_z = 2$ component. Thus, we can say that larger a produces amplification of small-scale structures. Next, we see what occurs when a becomes further large (u breaks up into small structures and spreads). In Figure 3.14, we show time evolution of the maximum values of $\Delta_y := |\partial_x^{-1}\partial_y^2 u/2|$, $\Delta_z := |\partial_x^{-1}\partial_z^2 u/2|$, $\Omega_y := |\partial_y u \partial_z \psi|$, and $\Omega_z := |\partial_z u \partial_y \psi|$, terms of the KPY equation. In the KP equation ($a = 0$), we obtain $\Delta_z = \Omega_y = \Omega_z = 0$ since the initial condition does not depend on z. In Figure 3.14(a) ($a = 0.1$), we observe $\Delta_y > \Delta_z$ and $\Omega_y > \Omega_z$ ($\partial_z u$ does not have a large value compared to $\partial_y u$). In Figure 3.14(b) ($a = 0.5$), we observe that values of Δ_z, Ω_y, Ω_z get close to that of Δ_y, although values of all components increase. In Figure 3.14(c) ($a = 0.8$), we observe that all of components have comparable values.

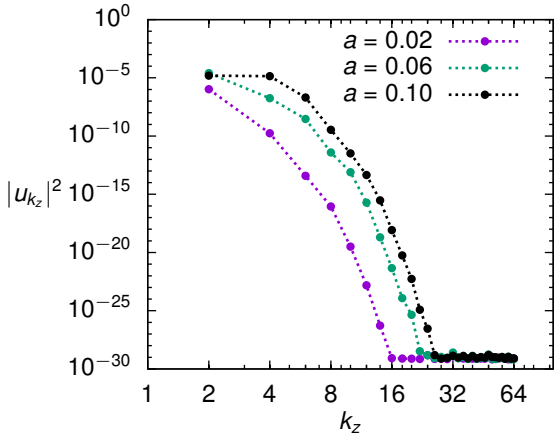

Figure 3.13: Spectrum $|u_{k_z}|^2$ for $a = 0.02, 0.06, 0.10$ ($\kappa = 2$ is fixed). The lowest Fourier component $k_z = 2$ has the largest value in the case of $a = 0.02$, but when the amplitude of the vortex field a increases, higher wavenumber components $k_z \geq 4$ increase greater than $k_z = 0.02$.

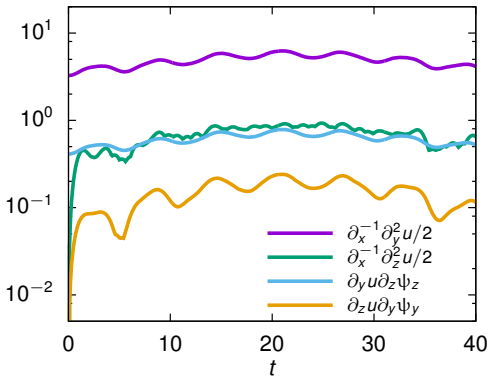

(a) $a = 0.1$

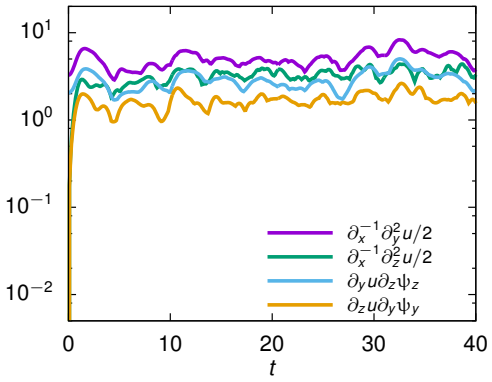

(b) $a = 0.5$

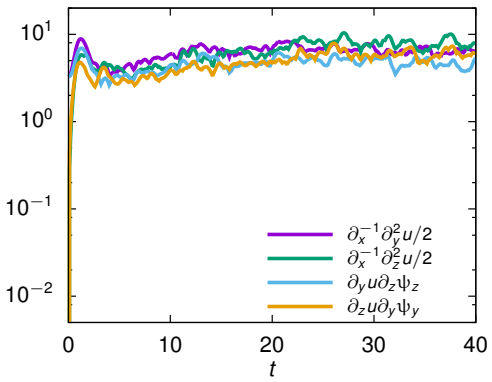

(c) $a = 0.8$

Figure 3.14: Time evolution of terms in the KPY equation. (a) When the amplitude of the vortex field is small, the maximum values of the terms $\Delta_z = |\partial_x^{-1}\partial_z^2 u/2|$ and $\Omega_z = |\partial_z u \partial_y \psi|$ are lower than those of $\Delta_y = |\partial_x^{-1}\partial_y^2 u/2|$ and $\Omega_y := |\partial_y u \partial_z \psi|$. (b) When the value of a increases, Δ_z and Ω_z increase greater than Δ_y and Ω_y, and (c) these terms have comparable amounts.

3.4 Conclusion

The newly formulated nonlinear system, derive in Chapter 2, describes the scattering of ion acoustic waves propagating in the ambient vortex field. In this chapter, we have investigated its integrability with theoretical and numerical analyses. First, we have executed the Painlevé test and elucidated that the vorticity introduces essential three-dimensionality to the wave, by which the integrability of the two-dimensional KP system is destroyed. Only in some strictly limited situation, the equation may be reduced to one- or two-dimensional integrable equations and passes the test.

Next, we have executed numerical simulation and observed effects of amplitudes and spatial scales of vortexes. When the amplitude is small, a two-dimensional line-soliton is deformed periodically but keep its solitary-wave structure. This result indicates that a two-dimensional line-soliton is stable near the zero-vorticity state, even though the evolution equation is non-integrable. The non-integrability (chaos) appears when the ambient vortex is strong; line-solitons break up into small scattered waves. We have clarified that growths of small-scale structures occur in the transition from periodic state to breaking state, and the amplitudes of y-dependent terms and z-dependent terms become comparable in the turbulent state.

Chapter 4

Bifurcation of Sheath Structures by Thermal Effects

In this chapter, we study the bifurcation of electrostatic sheath structures in the one-dimensional system due to thermal effects. We show the conceptual diagram of the system in Figure 4.1. We will start with a brief review of Bohm's equation without thermal effects. In Section 4.2, we include the adiabatic ion temperature and investigate changes in shapes of Sagdeev potentials and structures of electrostatic potentials (dashed arrows in Figure 4.1). We will find that the ion temperature suppresses the divergences of the first-order derivatives of Sagdeev potentials and brings about the possibility of bifurcation. In Section 4.3, we extend the system to include *heat flux* (wavy allows in Figure 4.1). This effect breaks the explicit relation between the ion temperature and the ion density, and we cannot write down the Sagdeev potential. We will find that the boundary condition of thermal transport equation (fixing the heat flux) controls the system and the temperature contrast changes depending on the ion Mach number and the value of the heat flux.

4.1 Brief review of Bohm's equation for cold ion

The basic equations are same as Chapter 2—the equation of continuity, the equation of motion, and the Poisson equation. We consider the one-dimensional system and steady state (ignoring time-derivatives). Then, we obtain the mass conservation law

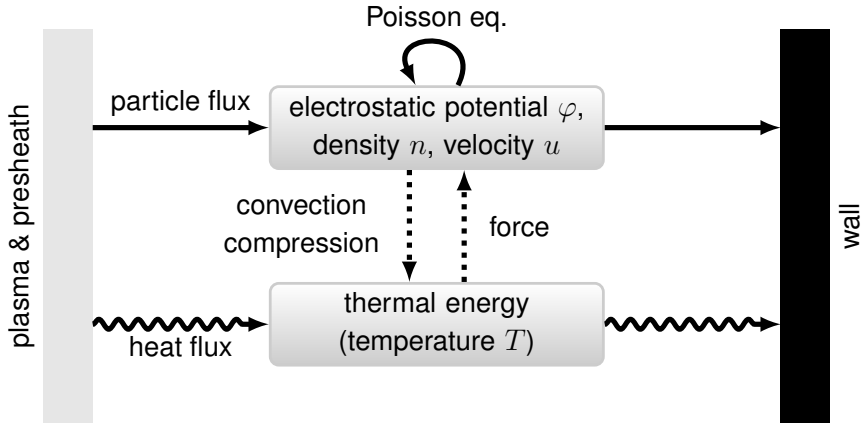

Figure 4.1: Conceptual diagram of the system. We include ion thermal energy (dashed arrows) in Section 4.2 and heat flux (wavy arrows) in Section 4.3. Thermal energy changes the sheath structure via the enthalpy term, and simultaneously ion flow transports thermal energy and increases it by compression heating.

$$nu = n_0 u_0 \tag{4.1}$$

from the equation of continuity and Bernoulli's law

$$\frac{1}{2}mu^2 + e\varphi = \frac{1}{2}mu_0^2 + \varphi_0 \tag{4.2}$$

from the equation of motion. The Poisson equation does not contain time-derivative:

$$-\varepsilon_0 \frac{\mathrm{d}^2\varphi}{\mathrm{d}x^2} = e(n - n_\mathrm{e}). \tag{4.3}$$

In these equations, symbols with subscript 0 denote the values at a reference point. We put the point on the boundary between sheath and plasma. Thus u_0 is the inflow ion velocity from the plasma to the wall and n_0 is the ion density of plasmas. We assume that the electron density obeys Boltzmann distribution with a constant temperature T_e and that quasi-neutrality is satisfied at the boundary. Thus we obtain $n_\mathrm{e} = n_0 \exp[e(\varphi - \varphi_0)/T_\mathrm{e}]$.

We use the ion sound speed without ion temperature $c_\mathrm{s} = \sqrt{T_\mathrm{e}/m}$ and the Debye

length $\lambda_{\mathrm{D}} = \sqrt{\varepsilon_0 T_{\mathrm{e}}/n_0 e^2}$ as the normalizing constants. The variables are normalized as followings: $\hat{x} = x/\lambda_{\mathrm{D}}$, $\hat{n} = n/n_0$, $\hat{u} = u/c_{\mathrm{s}}$, $\hat{\varphi} = e(\varphi - \varphi_0)/T_{\mathrm{e}}$. The normalized ion velocity at the boundary $\mathcal{M} = u_0/c_{\mathrm{s}}$ is a significant parameter in the following discussion. The mass conservation law and Bernoulli's law read as $\hat{n}\hat{u} = \mathcal{M}$ and $\hat{u}^2/2 + \hat{\varphi} = \mathcal{M}^2/2$. From these equations, we obtain the relation between the ion density and the electrostatic potential as

$$\hat{n} = \left(1 - \frac{2\hat{\varphi}}{\mathcal{M}^2}\right)^{-1/2} \tag{4.4}$$

under the condition $\hat{\varphi} \leq \mathcal{M}^2/2$. Substituting the equation into the Poisson equation, we obtain the Bohm equation:

$$\frac{\mathrm{d}^2\hat{\varphi}}{\mathrm{d}\hat{x}^2} = \mathrm{e}^{\hat{\varphi}} - \left(1 - \frac{2\hat{\varphi}}{\mathcal{M}^2}\right)^{-1/2}. \tag{4.5}$$

We may write the right-hand-side of the Bohm equation (4.5) as $-\partial V(\hat{\varphi})/\partial\hat{\varphi}$ with a potential function $V(\hat{\varphi})$.

$$V(\hat{\varphi}) = 1 - \mathrm{e}^{\hat{\varphi}} + \mathcal{M}^2\left[1 - \left(1 - \frac{2\hat{\varphi}}{\mathcal{M}^2}\right)^{1/2}\right], \tag{4.6}$$

where the integral constant is chosen as $V(0) = 0$. Thus, we may view the Bohm equation as the equation of motion for a pseudo-particle in the potential field $V(\hat{\varphi})$: $\mathrm{d}^2\hat{\varphi}/\mathrm{d}\hat{x}^2 = -\partial V(\hat{\varphi})/\partial\hat{\varphi}$ with the "position" $\hat{\varphi}$ and the "time" $\hat{x}$. The first usage of the pseudo-potential representation was by Sagdeev [64], and it is called the *Sagdeev potential*. We show two examples of the Sagdeev potential in Figure 4.2. The Sagdeev potential with $\mathcal{M} > 1$ has a local maximum value at $\hat{\varphi} = 0$ and that with $\mathcal{M} < 1$ has a minimum at the point.

The usage of Sagdeev potential helps us to solve the problem. For example, in the case of $\mathcal{M} > 1$, we see that electrostatic potential $\hat{\varphi}$ starts from the origin with a small gradient $\partial\hat{\varphi}/\partial x$ and monotonically drops. On the other hand, in the case of $\mathcal{M} < 1$, we see that electrostatic potential $\hat{\varphi}$ oscillates around the origin if that has a small gradient. The latter case is nothing but the linear ion acoustic waves.

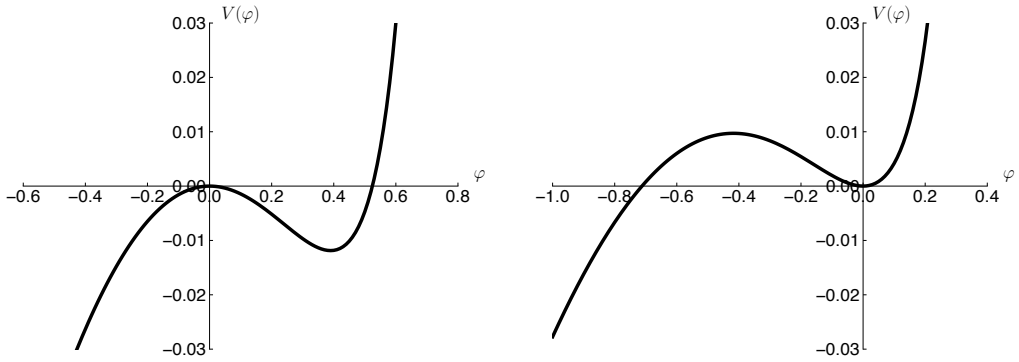

(a) $\mathcal{M} > 1$ (b) $\mathcal{M} < 1$

Figure 4.2: Examples of Sagdeev potential $V(\varphi)$. (b) The Sagdeev potential with $\mathcal{M} > 1$ has a local maximum value at $\varphi = 0$, and (b) that with $\mathcal{M} < 1$ has a minimum at the point.

Moreover, in the case of $\mathcal{M} > 1$, we can obtain a solution which starts from $\hat{\varphi} = 0$ to $\hat{\varphi} > 0$, bounces at a point with $V(\hat{\varphi}) = 0$, and goes back to $\hat{\varphi} = 0$. This is a solitary wave solution. Although we derive the Bohm equation with the assumption of steady states, we may boost the frame and obtain wave and soliton solutions. In fact, we also obtain Bohm's equation and the Sagdeev potential from the KdV equation (1.1) with assuming propagating waves ($u = u(x - vt)$), and the potential is identical to the one obtained by the perturbative expansion of the equation (4.6). Thus we may say that the Sagdeev potential connects analyses of solitons and electrostatic sheaths. We note that the first-order derivatives of Sagdeev potentials diverse at $\hat{\varphi} = \mathcal{M}^2/2$. This is caused by the fact that ions with initial velocity u_0 stop at the electrostatic potential with the value $\varphi = mu_0^2/2 + \varphi_0$ (see Bernoulli's law (4.2)).

4.2 New branches of electrostatic potentials created by thermal energy

4.2.1 Sagdeev potentials including adiabatic ion temperature

We include the ion thermal effect to Bernoulli's law (4.2):

$$\frac{1}{2}mu^2 + e\varphi + h = \frac{1}{2}mu_0^2 + e\varphi_0 + h_0, \tag{4.7}$$

where h is the ion enthalpy (h_0 is the ion enthalpy at the entrance of the sheath). Assuming that ion is an ideal gas, we write the enthalpy by the temperature as $h = c_\mathrm{p} T = (c_\mathrm{v} + 1)T$, where c_v is the heat capacity at constant volume and Meyer's relation $c_\mathrm{p} = c_\mathrm{v} + 1$ is used. We also assume that the heat capacity is that of a monatomic gas in a one-dimensional system: $c_\mathrm{v} = 1/2$.

We consider the governing equation of the ion temperature T. Here, we assume the adiabatic relation

$$T n^{-1/c_\mathrm{v}} = T_0 {n_0}^{-1/c_\mathrm{v}}. \tag{4.8}$$

We define normalized quantities as

$$\hat{T} = \frac{T}{T_\mathrm{e}}, \qquad \hat{T}_0 = \frac{T_0}{T_\mathrm{e}}. \tag{4.9}$$

Not only the inflow velocity $\mathcal{M}$, but also the inside temperature $\hat{T}_0$ is a significant parameter in the following analysis.

From Bernoulli's law (4.7) and the adiabatic relation (4.8), we obtain

$$\hat{u}^4 - \mathcal{M}^2 \left(1 + \frac{3\hat{T}_0}{\mathcal{M}^2} - \frac{2\hat{\varphi}}{\mathcal{M}^2} \right) \hat{u}^2 + 3\hat{T}_0 \mathcal{M}^4 = 0. \tag{4.10}$$

Under the condition

$$\hat{\varphi} \leq \hat{\varphi}_* = \frac{\mathcal{M}^2}{2} \left(1 - \frac{\sqrt{3\hat{T}_0}}{\mathcal{M}} \right)^2, \tag{4.11}$$

the equation (4.10) has two real solutions of $\hat{u}$:

$$\hat{u}_\pm(\hat{\varphi}) = \frac{\mathcal{M}}{2} \left(\sqrt{A_+^2 - \frac{2\hat{\varphi}}{\mathcal{M}^2}} \pm \sqrt{A_-^2 - \frac{2\hat{\varphi}}{\mathcal{M}^2}} \right) \tag{4.12}$$

with

$$A_\pm = 1 \pm \frac{\sqrt{3\hat{T}_0}}{\mathcal{M}}. \tag{4.13}$$

Then, the Bohm equation becomes

$$\frac{\mathrm{d}^2 \hat{\varphi}}{\mathrm{d}\hat{x}^2} = \mathrm{e}^{\hat{\varphi}} - \frac{\mathcal{M}}{\hat{u}_\pm(\hat{\varphi})} \tag{4.14}$$

and its right-hand-side may be expressed with the Sagdeev potential

$$V_\pm(\hat{\varphi}) = -\mathrm{e}^{\hat{\varphi}} + \frac{\mathcal{M}^3}{6\sqrt{3\hat{T}_0}} \left[-\left(A_+^2 - \frac{2\hat{\varphi}}{\mathcal{M}^2} \right)^{3/2} \pm \left(A_-^2 - \frac{2\hat{\varphi}}{\mathcal{M}^2} \right)^{3/2} \right] + C_\pm. \tag{4.15}$$

We find that the values of two solutions $\hat{u}_\pm(\hat{\varphi})$ (and the values of $V_\pm$) coincide at the point $\hat{\varphi} = \hat{\varphi}_* = (\mathcal{M}^2/2)A_-^2$. However, $V'_\pm$ is *not* Lipschitz continuous at the point. Thus, the solution of the equation (4.14) loses its uniqueness (see Appendix A.4), and the solution can bifurcate from one of the Sagdeev potentials $V_\pm$ to the other. We define the integral constants to satisfy $V_+(0) = 0$ and $V_+(\hat{\varphi}_*) = V_-(\hat{\varphi}_*)$.

We note that the existence of multiple Sagdeev potentials is already known, e.g. in Ref. [4]. However, it must be highlighted because it is difficult to construct solutions without generalizing boundary condition and using Lipschitz discontinuity. Here, we show one possibility of constructing an asymptotic solution without using these tools later (Class (F) of Section 4.2.2).

4.2.2 Solutions of Bohm's equation

In this section, we solve the Bohm equation (4.14) on the one-dimensional space $\hat{x} \in (-\infty, 0]$. We consider that the wall is placed at $x = 0$ and $x \to -\infty$ is the plasma region, and set the boundary condition as

$$\hat{\varphi}(0) = -P, \qquad \lim_{n\to\infty} \hat{\varphi}(\hat{x}_n) = 0, \tag{4.16}$$

where P is the normalized value of the electric potential difference between the plasma and the wall, and $\{\hat{x}_n\}$ is a certain sequence satisfying $\lim_{n\to\infty} \hat{x}_n \to -\infty$. Without normalizing (remembering $\hat{\varphi} = e(\varphi - \varphi_0)/T_\mathrm{e}$), this boundary condition reads as

$$\varphi(0) = 0, \qquad \lim_{n\to\infty} \varphi(x_n) = \varphi_0 = \frac{T_\mathrm{e}}{e} P. \tag{4.17}$$

The second boundary condition is "weak" one proposed by Yoshida and Yamada [90], which indicates that the value of the electrostatic potential φ may oscillate around the limit value P but should not deviate from it. This generalization, including the asymptotic boundary condition $\lim_{x\to-\infty} \hat{\varphi}(\hat{x}) = 0$, enables us to obtain a variety of solutions.

Bohm's criterion is necessary for the existence of asymptotic solutions, and conditions of the "height" of the Sagdeev potential is required for the existence of oscillatory solutions. However, even if we cannot construct the solution satisfying boundary conditions only in one of the potentials $V_{\pm}$, we may construct the solution by using the bifurcation due to the Lipschitz discontinuity. According to the values of $\mathcal{M}$ and $\hat{T}_0$, the shape of Sagdeev potential $V_{\pm}(\varphi)$ changes.

We classify them and show as Figure 4.3. (In the rest of the section, we omit the hat $\hat{}$ for simplicity.) The separations expressed by dashed lines are determined by $\mathcal{M} \gtrless \sqrt{1+3T_0}$ and $\mathcal{M} \gtrless \sqrt{3T_0}$. The former corresponds to nothing but Bohm's criterion defined by $V_+''(0) \leq 0$, and the latter switches between $V_+'(0) = 0$ and $V_-'(0) = 0$. The colored separations are defined by heights of the Sagdeev potentials. We also consider two important points of φ. One is $\varphi = \varphi_*$ defined in the equation (4.11). This is the edge points of the Sagdeev potentials and may be the bifurcation point. The other is defined by $V_+'(\varphi) = 0$ and $V_+''(\varphi) < 0$, and we denote by φ_{**}. Its value changes according to the condition $\mathcal{M} \gtrless \sqrt{1+3T_0}$; $\mathcal{M} > \sqrt{1+3T_0}$ leads to $\varphi_{**} = 0$ and $\mathcal{M} < \sqrt{1+3T_0}$ leads to $\varphi_{**} < 0$. (The latter is expressed by the Lambert W function, which is not an elementary function [16].) These rules are summarized in Table 4.1.

We now describe the Sagdeev potentials and solutions in each class.

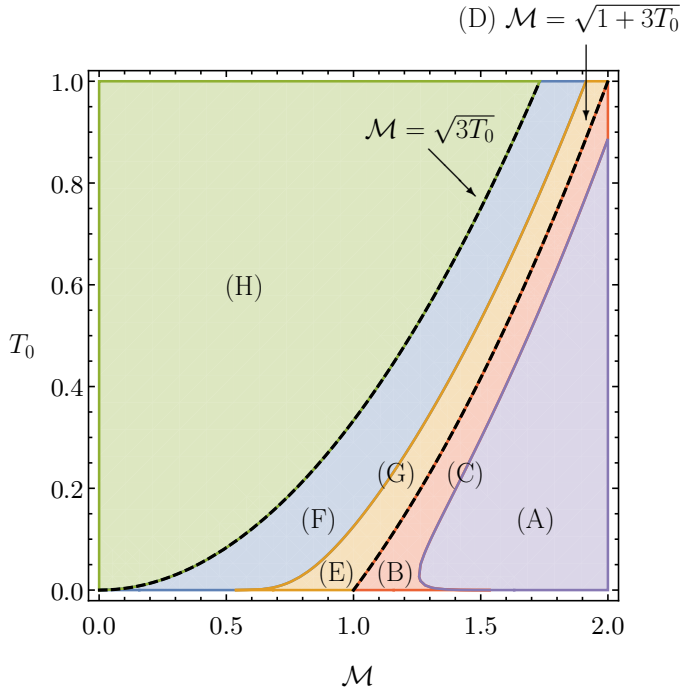

Figure 4.3: Classification of the Sagdeev potentials with respect to the values of the normalized ion velocity $\mathcal{M}$ and the normalized ion temperature T_0.

Table 4.1: Classification rules of the Sagdeev potentials in Figure 4.3 and constructible solutions (a: asymptotic ones, o: oscillatory ones, b: oscillatory ones bifurcated from V_- to V_+; * denotes that a constraint for the value of P is required).

	$V'(0)=0$	$V''(0) \gtrless 0$	$V(\varphi_*) \gtrless V(\varphi_{**})$	solution
(A)	$V_+'(0)=0$	$V_+''(0)<0$	$V_+(\varphi_*)<V_+(0)$	a
(B)	$V_+'(0)=0$	$V_+''(0)<0$	$V_+(\varphi_*)>V_+(0)$	a/o
(C)	$V_+'(0)=0$	$V_+''(0)<0$	$V_+(\varphi_*)=V_+(0)$	a/o/b
(D)	$V_+'(0)=0$	$V_+''(0)=0$	——	a
(E)	$V_+'(0)=0$	$V_+''(0)>0$	$V_+(\varphi_*)>V_+(\varphi_{**})$	o
(F)	$V_+'(0)=0$	$V_+''(0)>0$	$V_+(\varphi_*)<V_+(\varphi_{**})$	o*/b
(G)	$V_+'(0)=0$	$V_+''(0)>0$	$V_+(\varphi_*)=V_+(\varphi_{**})$	o/b
(H)	$V_-'(0)=0$	$V_-''(0)<0$	——	a

Class A: $V_+'(0) = 0$, $V_+''(0) < 0$, $V_+(\varphi_*) < V_+(0)$. We show an example of Sagdeev potential for the class (A) in Figure 4.4(a). We can construct asymptotic solutions in V_+ as Figure 4.4(b). We cannot construct oscillatory solutions because $V_+(0) > V_+(\varphi_*) = V_-(\varphi_*)$ is satisfied.

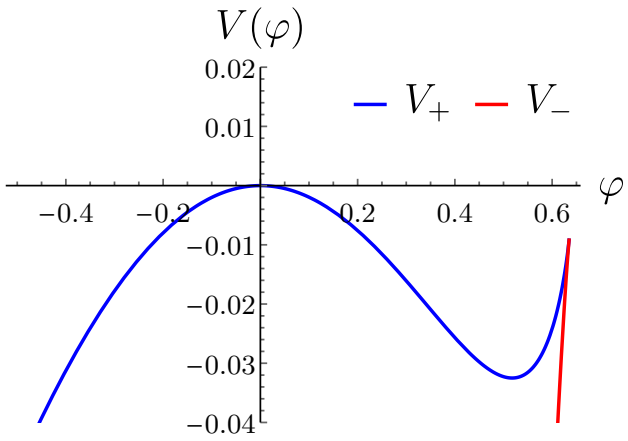

(a)

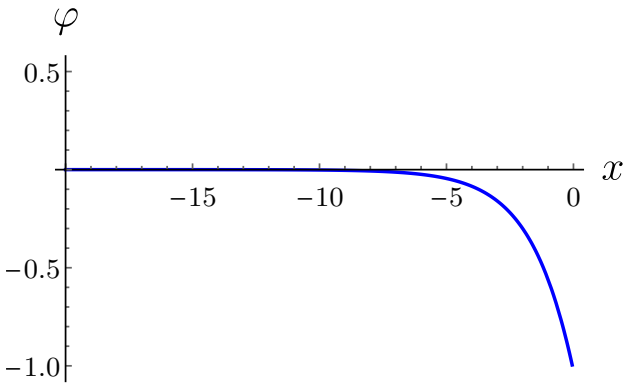

(b)

Figure 4.4: (a) Sagdeev potential and (b) an example of solutions for class (A). We can construct only asymptotic solutions.

Class (B): $V_+'(0) = 0$**,** $V_+''(0) < 0$**,** $V_+(\varphi_*) > V_+(0)$**.** We show an example of Sagdeev potential for the class (B) in Figure 4.5(a). In addition to asymptotic solutions like Figure 4.4(b), we can also obtain oscillatory solutions in V_+ as Figure 4.5(b). Solutions bifurcated from V_- to V_+ cannot exist because of $V_+(\varphi_*) = V_-(\varphi_*) > V_+(0)$

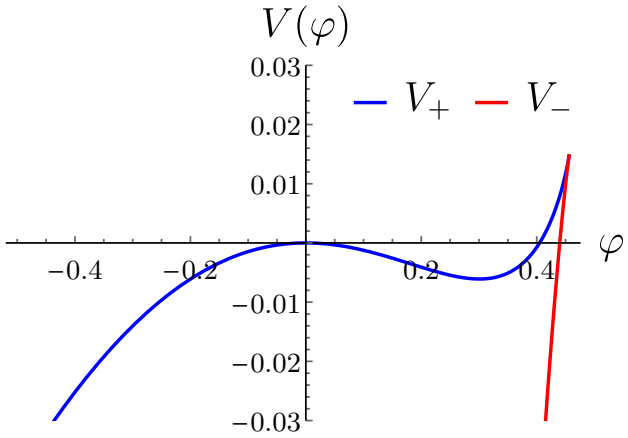

(a)

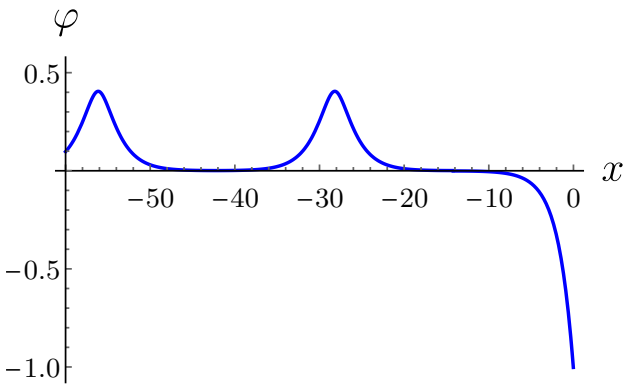

(b)

Figure 4.5: (a) Sagdeev potential and (b) an example of solutions for class (B). We can construct both of asymptotic and oscillatory solutions.

Class (C): $V_+'(0) = 0$**,** $V_+''(0) < 0$**,** $V_+(\varphi_*) = V_+(0)$**.** We show an example of Sagdeev potential for the class (C) in Figure 4.6(a). This class is on the boundary between class (A) and (B). We can construct both of asymptotic and oscillatory solutions in V_+ such as Figures 4.4(b) and 4.5(b), and we also can construct oscillatory solutions bifurcated from V_- to V_+ as Figure 4.6(b).

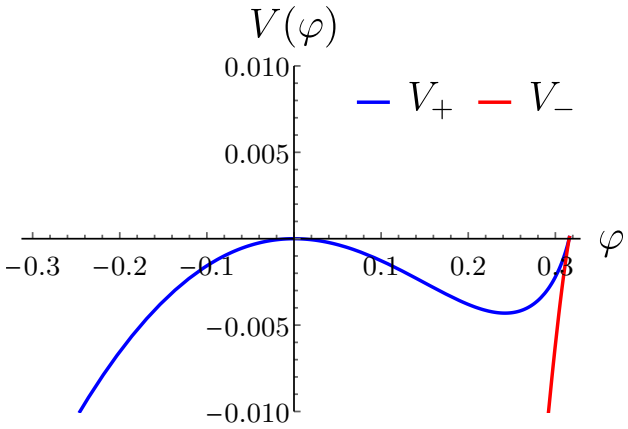

(a)

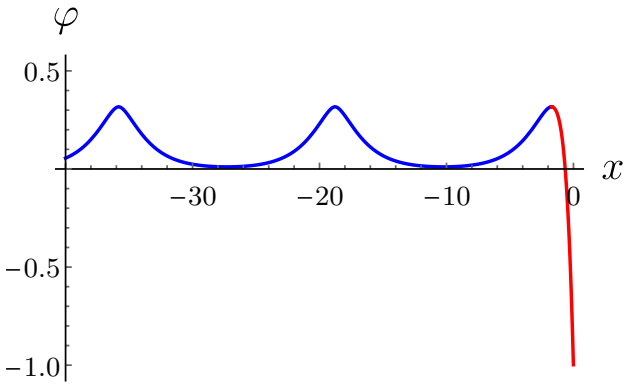

(b)

Figure 4.6: (a) Sagdeev potential and (b) an example of solutions for class (C). We can construct both of asymptotic and oscillatory solutions on V_+, and also oscillatory solutions bifurcated from V_- to V_+.

Class (D): $V'_+(0) = 0$**,** $V''_+(0) = 0$**.** We show an example of Sagdeev potential for the class (D) in Figure 4.7. In this class, $\mathcal{M} = \sqrt{1 + 3T_0}$ is satisfied and $V''_+(0) = 0$. Since there are no points with $V''_+(\varphi) < 0$, we can only construct an asymptotic solution like Figure 4.4(b).

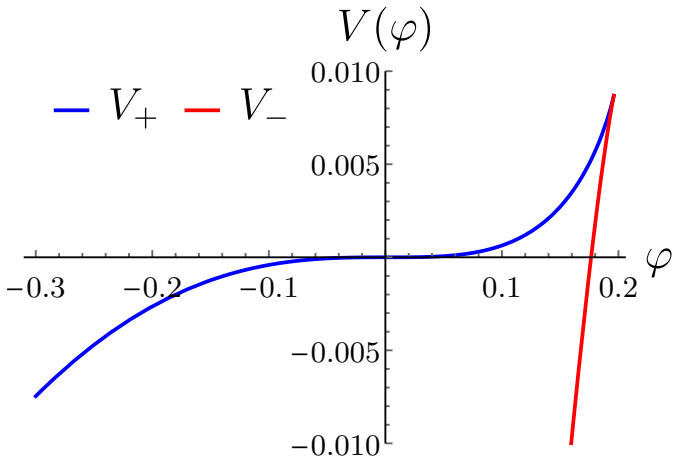

Figure 4.7: Sagdeev potential for class (D). There are no points with $V''_+(\varphi) < 0$, and we can only construct asymptotic solutions.

Class (E): $V_+'(0) = 0$, $V_+''(0) > 0$, $V_+(\varphi_*) > V_+(\varphi_{**})$. We show an example of Sagdeev potential for the case (E) in Figure 4.8(a). The top of $V_+(\varphi)$ is lower than that of $V_-(\varphi)$. In this class, we can only construct oscillatory solutions in the Sagdeev potential V_+ as Figure 4.8(b). It should be noted that some dissipative mechanisms are necessary.

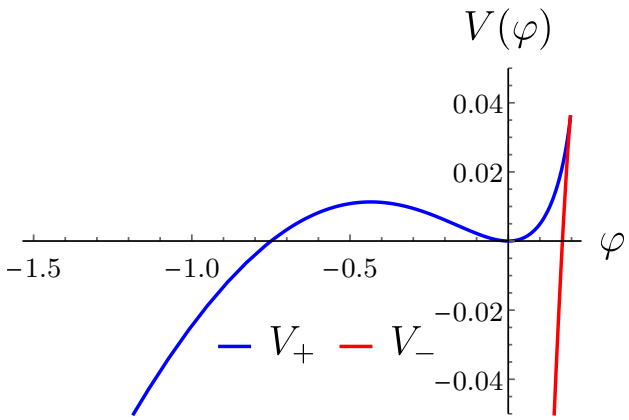

(a)

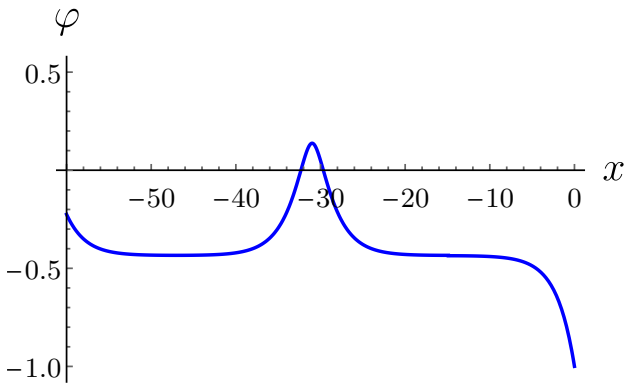

(b)

Figure 4.8: (a) Sagdeev potential and (b) an example of solutions for class (E). We can only construct oscillatory solutions in the Sagdeev potential V_+.

Class (F): $V_+'(0) = 0$, $V_+''(0) > 0$, $V_+(\varphi_*) < V_+(\varphi_{**})$. We show an example of Sagdeev potential for the case (F) in Figure 4.9(a). The top of $V_-(\varphi)$ is higher than that of $V_-(\varphi)$. Thus we cannot construct the solution only in V_+ unless we choose a proper value of P [90], but we can construct oscillatory solutions bifurcated from V_- to V_+ as Figure 4.9(b). In this case, any dissipative mechanisms are not necessary.

Class (G): $V_+'(0) = 0$, $V_+''(0) > 0$, $V_+(\varphi_*) = V_+(\varphi_{**})$. Class (G) is the boundary between classes (E) and (F). Both of oscillatory solutions on V_+ (Figure 4.8(b)) and ones bifurcated from V_- to V_+ (Figure 4.9(b)) may exist.

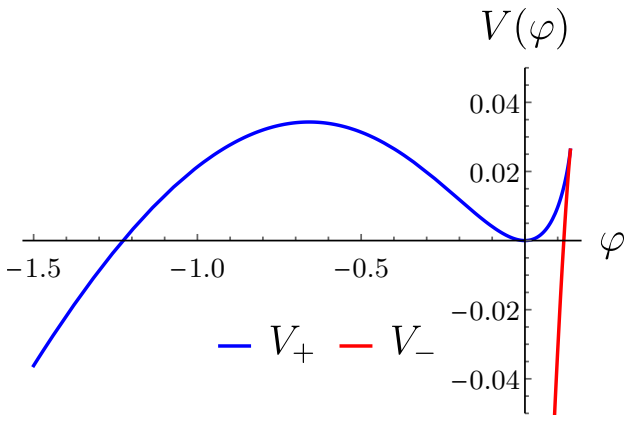

(a)

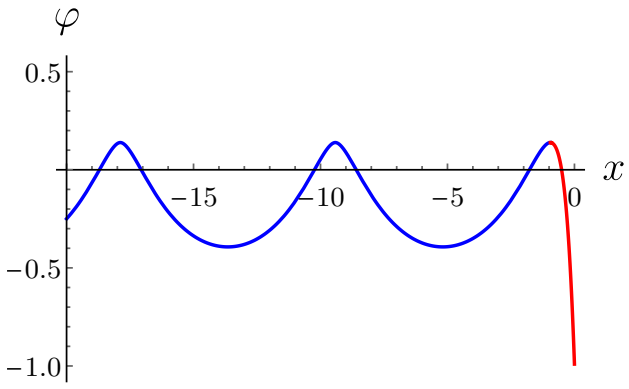

(b)

Figure 4.9: (a) Sagdeev potential and (b) an example of solutions for class (F). We can only construct oscillatory solutions bifurcated from V_- to V_+.

Class (H): $V'_-(0) = 0$**,** $V''_-(0) < 0$**.** We show an example of Sagdeev potential for the class (H) in Figure 4.10(a). This is the only one possibility to obtain asymptotic solutions as Figure 4.10(b) in V_- without using weak boundary conditions.

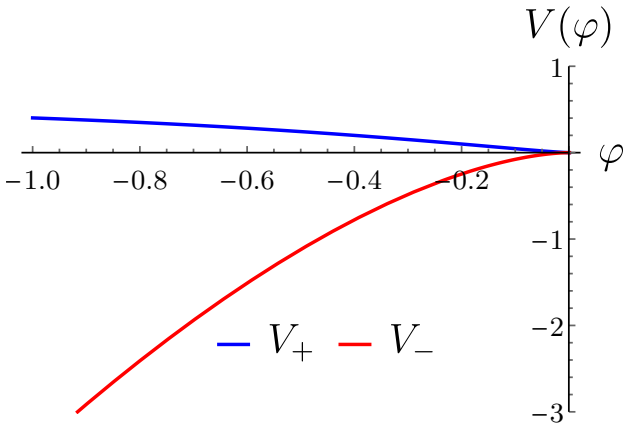

(a)

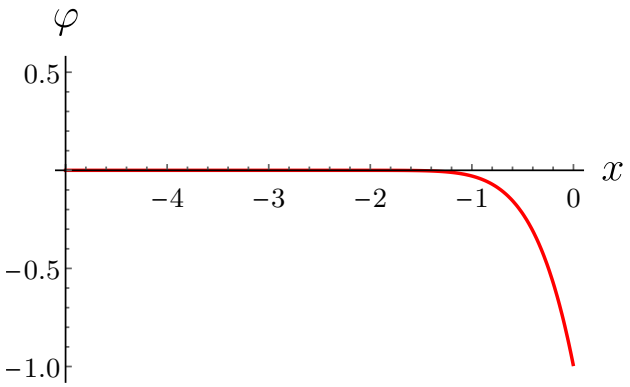

(b)

Figure 4.10: (a) Sagdeev potential and (b) an example of solutions for class (H). We can construct asymptotic solutions in V_-.

We remark on the determination of the difference of electrostatic potential P between plasma and wall. In this section, we have focused on structures of solutions created in each parameter regions, and we have assumed $P = 1$ for simplicity. In addition, if we choose a proper value of P, we can obtain a special oscillatory solution for classes (E) and (F). However, we cannot determine the value of P arbitrarily in practice—it is self-regulated by interactions between plasmas and walls. In the analysis of the next section, we will use a relation between potential difference and ion velocity known as the floating potential.

4.3 Thermal diffusion in sheath structure

The analysis of the previous section, we assume the adiabatic property for the ion temperature (4.8). In this section, we generalize the relation and introduce a thermal diffusion effect. This generalization breaks the explicit relation between the ion temperature and the ion density, and we cannot express a Sagdeev potential in the Poisson equation (Bohm equation).

4.3.1 Non-adiabatic ion temperature effect

We write down a differential equation for ion temperature and compose a system of equations. The equation of temperature is derived from the first law of thermodynamics $\mathrm{d}E = -p\,\mathrm{d}V + \delta Q = p/n^2\,\mathrm{d}n + \delta Q$. Let us assume the relation for ideal gas $E = c_\mathrm{v}T$, then the first law reads to

$$c_\mathrm{v} n \frac{\mathrm{d}T}{\mathrm{d}t} + p(\nabla \cdot \boldsymbol{u}) = n\dot{Q},$$

where we use the equation of continuity $\mathrm{d}n/\mathrm{d}t = -n(\nabla\cdot\boldsymbol{u})$. The heat $\dot{Q}$ may contain any irreversible effects. Here we put $n\dot{Q} = -\nabla \cdot \boldsymbol{F}$ with a heat flux $\boldsymbol{F}$ and assume that $\boldsymbol{F}$ obeys Fourier's law $\boldsymbol{F} = -k\nabla T$ (k: thermal conductivity).

Considering the one-dimensional system and steady states, we obtain

$$nu\frac{\partial T}{\partial x} + \frac{nT}{c_\mathrm{v}}\frac{\partial u}{\partial x} = -\frac{1}{c_\mathrm{v}}\frac{\partial F}{\partial x} \tag{4.18}$$

The normalization of the ion temperature is same as previous section (4.9): $\hat{T} = T/T_\mathrm{e}$. Then we obtain

$$\hat{n}\hat{u}\frac{\partial \hat{T}}{\partial \hat{x}} + \frac{\hat{n}\hat{T}}{c_\mathrm{v}}\frac{\partial \hat{u}}{\partial \hat{x}} = -\frac{1}{c_\mathrm{v}}\frac{\partial}{\partial \hat{x}}\left(\frac{F}{c_\mathrm{s} n_0 T_\mathrm{e}}\right), \tag{4.19}$$

and normalize the heat flux as

$$\hat{F} = \frac{F}{n_0 c_\mathrm{s} T_\mathrm{e}} = -\frac{\partial}{\partial \hat{x}}\left(\frac{k}{\lambda_\mathrm{D} n_0 c_\mathrm{s}}\frac{T}{T_\mathrm{e}}\right). \tag{4.20}$$

We define the thermal diffusivity χ as $\chi = k/c_\mathrm{v} n_0$, and normalize it as $\hat{\chi} = \chi/c_\mathrm{s}\lambda_\mathrm{D}$. We may express the normalization of heat flux as $\hat{F} = -c_\mathrm{v}\hat{\chi}\partial\hat{T}/\partial\hat{x}$.

Now we write the system of equations, omitting the hat $\hat{}$ for simplicity. The differential equation for the ion temperature (4.19) reads as

$$\chi\frac{\partial^2 T}{\partial x^2} - \mathcal{M}\frac{\partial T}{\partial x} - \frac{\mathcal{M}}{c_\mathrm{v}}\frac{\partial(\ln u)}{\partial x}T = 0, \tag{4.21}$$

where the mass conservation law $nu = \mathcal{M}$ is used. From Bernoulli's law, we obtain the relation among the ion velocity, the electrostatic potential, and the ion temperature as

$$u = \mathcal{M}\left[1 - \frac{2\varphi}{\mathcal{M}^2} - \frac{2c_\mathrm{p}}{\mathcal{M}^2}(T - T_0)\right]^{1/2}. \tag{4.22}$$

Finally, the Poisson equation is

$$\frac{\partial^2 \varphi}{\partial x^2} = \mathrm{e}^{\varphi} - \left[1 - \frac{2\varphi}{\mathcal{M}^2} - \frac{2c_\mathrm{p}}{\mathcal{M}^2}(T - T_0)\right]^{-1/2}, \tag{4.23}$$

where the mass conservation law $nu = \mathcal{M}$ and the equation (4.22) are used.

In the limit to the pure thermal diffusion, ignoring the ion velocity in equation (4.21), we obtain $\partial_x F = 0$ and $F = -c_\mathrm{v}\chi\partial_x T$ leads to the linear distribution $\partial_x T = \text{const}$. In next section, we solve the system (4.21)–(4.23) and compare results of temperature to the linear distribution (for pure thermal diffusion without ion velocity).

In the opposite limit to $k \to 0$, the equation (4.21) leads to $c_\mathrm{v} u\partial_x T + T\partial_x u = 0$, and we obtain the adiabatic relation $Tn^{-1/c_\mathrm{v}} = T_0 n_0^{-1/c_\mathrm{v}}$ using the mass conservation law $nu = \mathcal{M}$. It should be noted that this limit causes problems of the *singular*

perturbation, since the order of differential equation is changed. We must set two boundary conditions for equation (4.21), but we can apply only one boundary condition to the equation $\partial_x \ln(Tu^{1/c_\mathrm{v}}) = 0$.

4.3.2 Numerical analysis

We execute numerical analysis of the equations (4.21)–(4.23) on the one-dimensional space $x \in [0, L]$. We consider that the wall is placed at $x = L = 10$ and $x = 0$ is the inside edge of the sheath.

4.3.2.1 Boundary condition

We put the boundary conditions of the ion temperature as followings. At the wall boundary $x = L$ $(= 10)$, we assume that the ion temperature is fixed to a value T_w. Here we put $T_\mathrm{w} = 0.1$. We use two types of boundary conditions at the inside boundary $x = 0$ and compare them. One is to control the heat flux into the system F_in (we call flux-driven condition), and the other is to control the ion temperature T_in (we call temperature-driven condition). Since we use Fourier's law for the heat flux, the former is the Neumann boundary condition, and the latter is the Dirichlet boundary condition.

We set the basis of φ at the inside edge of sheath region ($\varphi(0) = 0$), and consider the boundary value at the wall side φ_w as following, which is called *floating potential* [68]. We assume that the wall is floating and the electrical current at its surface is zero. The ion current is expressed as $J_\mathrm{i} = en_0u_0$, where we use the mass conservation law (4.1), and the electron current is expressed as $J_\mathrm{e} = -en_0\sqrt{T_\mathrm{e}/2\pi m_\mathrm{e}}\mathrm{e}^{-e\varphi_\mathrm{w}/T_\mathrm{e}}$ (we use non-normalized symbols). Then, the condition $J_\mathrm{i} + J_\mathrm{e} = 0$ leads to

$$\begin{aligned} \frac{e\varphi_\mathrm{w}}{T_\mathrm{e}} &= -\frac{1}{2}\ln\left(\frac{m}{2\pi m_\mathrm{e}}\right) + \ln\left(\frac{u_0}{c_\mathrm{s}}\right) \qquad \text{(non-normalized form)}, \\ \varphi_\mathrm{w} &= -\frac{1}{2}\ln\left(\frac{m}{2\pi m_\mathrm{e}}\right) + \ln\mathcal{M} \qquad \text{(normalized form)}. \end{aligned} \tag{4.24}$$

We use $m = 1.67 \times 10^{-27}\,\mathrm{kg}$ (proton mass) and $m_\mathrm{e} = 9.11 \times 10^{-31}\,\mathrm{kg}$, and plot the

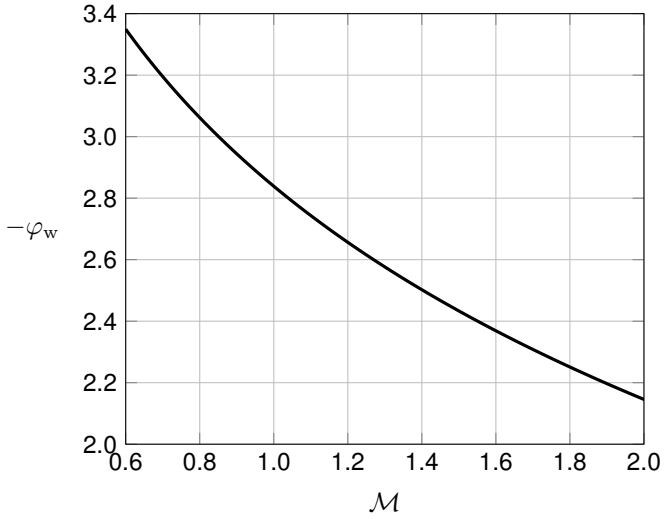

Figure 4.11: Relation between the ion velocity $\mathcal{M}$ and the floating potential φ_w (4.24)

relation (4.24) in Figure 4.11.

For comparison, we show the solution of the Bohm equation (4.5) without ion temperature effects under the boundary condition defined by the floating potential (4.24) in Figure 4.12. Compared to the result of $\mathcal{M} = 1$ (Bohm's criterion), that $\mathcal{M} = 0.85$ has a larger gradient. The former corresponds to the asymptotic solution, and the latter corresponds to the oscillatory solution.

4.3.2.2 Numerical procedure

The system of equations (4.21)–(4.23) are solved as following: (i) we solve the Poisson equation (4.23) with the initial condition $T = T_0$; (ii) we express the ion velocity with equation (4.22) and solve the temperature equation (4.21); (iii) we solve the Poisson equation (4.23) with updated temperature T; (iv) we return to (ii) unless the difference between old and updated profiles is small. We show the diagram in Figure 4.13.

We have two control parameters. One is the boundary value of heat flux or temperature and the other is the ion inflow velocity. In order to investigate the

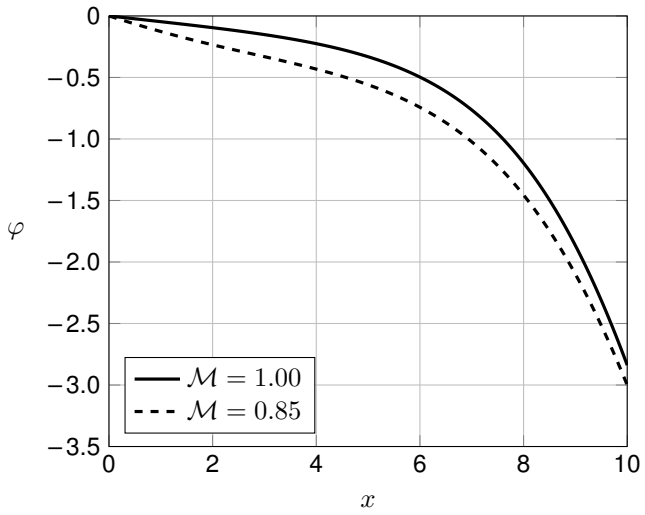

Figure 4.12: Comparison between electrostatic potentials for $\mathcal{M} = 1$ and $\mathcal{M} = 0.85$. The latter has a large gradient compared to the former.

relation between the electrostatic potential structures and the thermal diffusion, we use a Mach number with a finite ion temperature

$$\tilde{\mathcal{M}} = \frac{\mathcal{M}}{\sqrt{1 + 3T_0}} \tag{4.25}$$

as a control parameter instead of $\mathcal{M}$ (Bohm's criterion is $\tilde{\mathcal{M}} = 1$). In the following numerical analysis, the values of the inside ion temperature T_0 is controlled by the boundary condition. Especially, in the analysis of the flux-driven condition, the value of T_0 may change in the iteration process. We fix the value of $\tilde{\mathcal{M}}$ and modify the value of $\mathcal{M}$ according to the relation (4.25). We note that this modification also affects the value of floating potential (4.24).

4.3.2.3 Numerical results

We show the results of the flux-driven condition in Figure 4.14. Figure 4.14(a) is the temperature distribution with $\tilde{\mathcal{M}} = 1$ and $F_{\rm in} = 0.14$. We observe that the temperature contrast between boundaries is larger than that of the linear distribution (pure diffusion without ion velocity). Figure 4.14(b) is the temperature distribution with $\tilde{\mathcal{M}} = 0.85$ and $F_{\rm in} = 0.08$. In this case, we observe that the temperature contrast

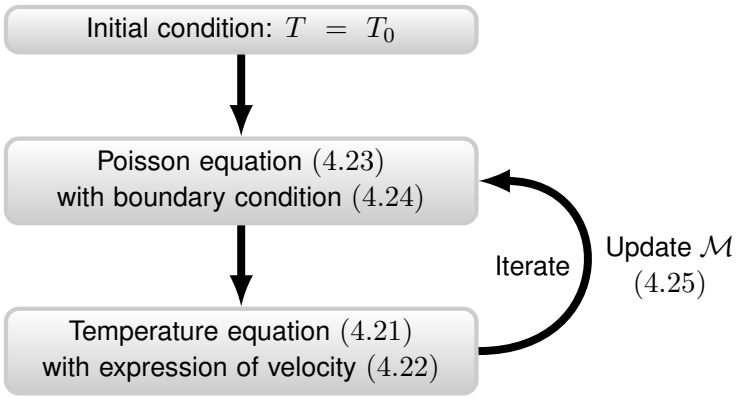

Figure 4.13: A diagram of the numerical procedure. The Poisson equation (4.23) and the temperature equation (4.21) are solved iteratively. The value of $\mathcal{M}$ is changed according to the equation (4.25) with fixing the value of $\tilde{\mathcal{M}}$.

between boundaries is smaller than that of the linear distribution.

Next, we show the results of the temperature-driven condition in Figure 4.15. Figure 4.15(a) is the temperature distribution with $\tilde{\mathcal{M}} = 1$ and $T_{\rm in} = 0.5$. We observe that temperature distributes above that of the linear distribution. We also observe that the heat flux (the temperature gradient) at the sheath edge ($x = 0$) is smaller than that of the linear distribution. In the result with $\tilde{\mathcal{M}} = 0.85$ and $F_{\rm in} = 0.3$, shown in Figure 4.15(b), the above results are reversed.

Since we cannot express the relation between ion temperature and ion density, the exact condition of sheath criterion is unclear. We show the results of electrostatic potential in Figure 4.16. Comparing them to Figure 4.12—the solution of Bohm's equation without ion temperature under the same boundary condition—we can say that $\tilde{\mathcal{M}} = 1$ corresponds to an asymptotic solution and $\tilde{\mathcal{M}} = 0.85$ corresponds to an oscillatory solution.

From these results, we can say that potential structures with $\tilde{\mathcal{M}} = 1$ increase temperature contrast in the flux-driven system and reduce flux in the temperature-driven system. On the other hand, potential structures with $\tilde{\mathcal{M}} = 0.85$ decrease temperature contrast in the flux-driven system and increase flux in the temperature-

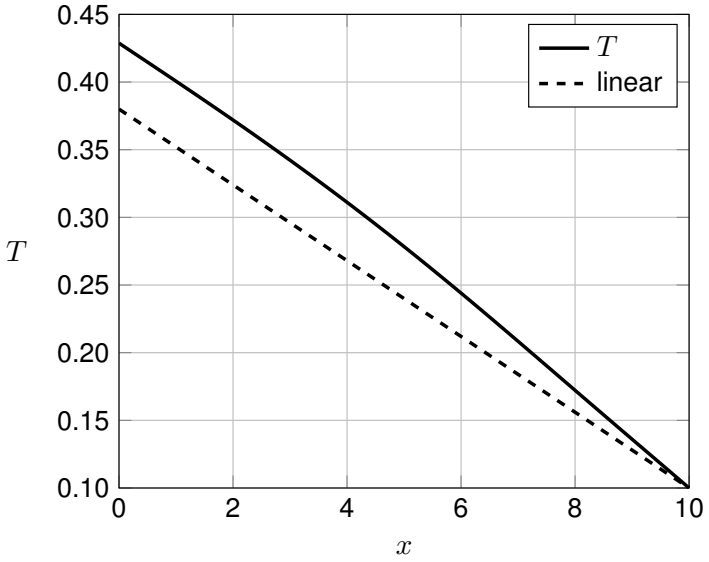

(a) $\tilde{\mathcal{M}} = 1$, $F_{\rm in} = 0.14$: the temperature contrast is larger than that of the linear distribution

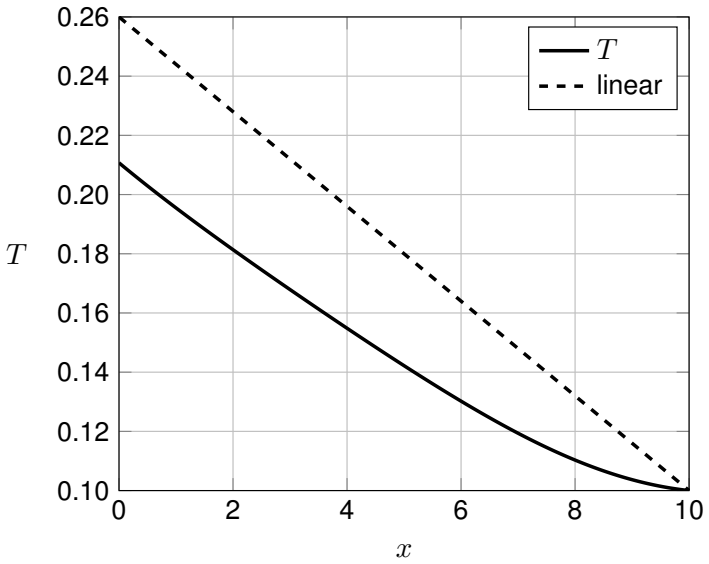

(b) $\tilde{\mathcal{M}} = 0.85$, $F_{\rm in} = 0.08$: the temperature contrast is smaller than that of the linear distribution

Figure 4.14: Temperature distribution in the flux-driven system with $\chi = 10$, compared to the linear distribution.

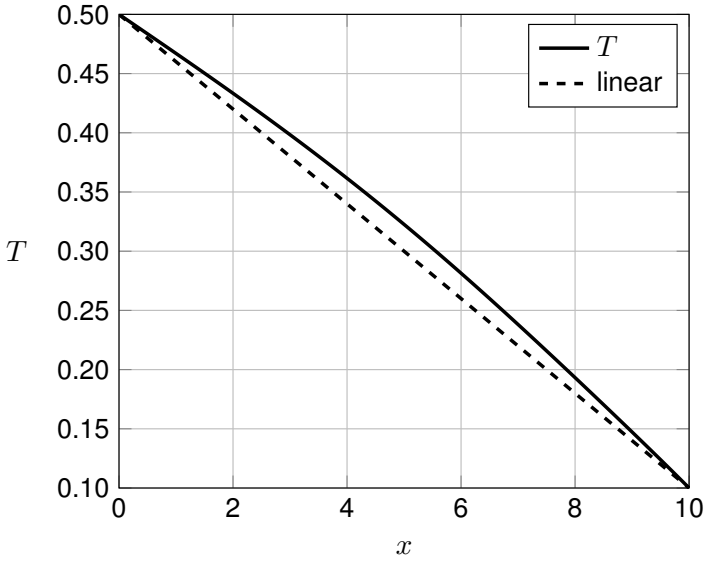

(a) $\tilde{\mathcal{M}} = 1$, $T_{\text{in}} = 0.5$: the inside temperature gradient is smaller than that of the linear distribution

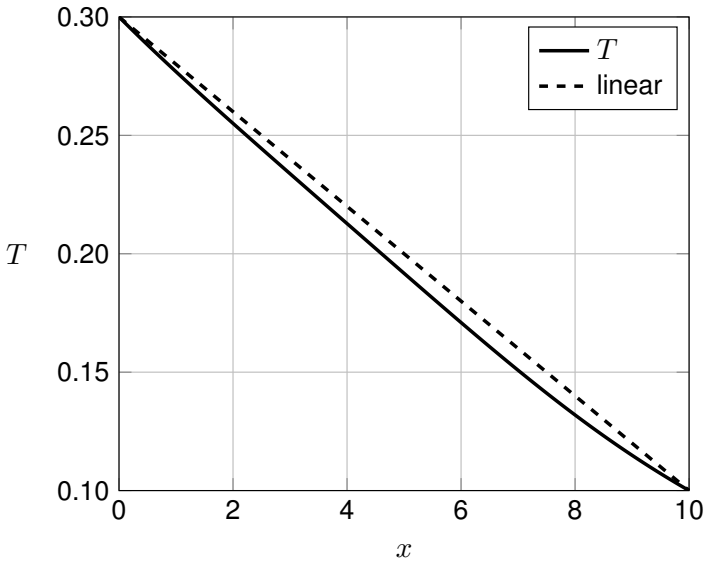

(b) $\tilde{\mathcal{M}} = 0.85$, $T_{\text{in}} = 0.3$: the inside temperature gradient is larger than that of the linear distribution

Figure 4.15: Temperature distribution in the temperature-driven system with $\chi = 10$, compared to the linear distribution.

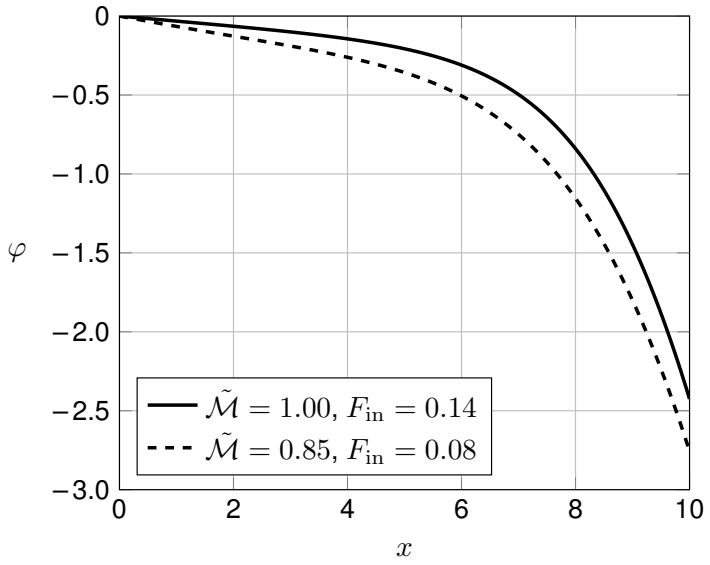

(a) Flux-driven systems

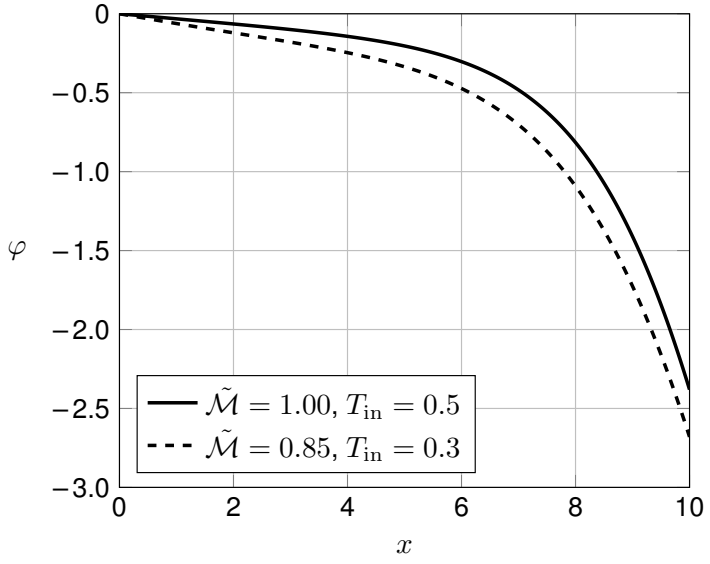

(b) Temperature-driven systems

Figure 4.16: The distribution of electrostatic potentials. In both of flux-driven and temperature-driven systems, the gradient takes a large value in the case of $\tilde{\mathcal{M}} = 0.85$ compared to $\tilde{\mathcal{M}} = 1$. The distributions are rarely different from those in Figure 4.12 (without ion temperature effect).

driven system.

In order to clarify the condition of these transitions occurs, we show the differences between the flux [temperature] at the inside edge $F_{\rm in}$ [$T_{\rm in}$] and those of the linear distribution (thermal diffusion without ion flow) $F_{\rm diff}$ [$T_{\rm diff}$] with changing the values of control parameters in Figure 4.17. Dashed lines indicate points where they coincide. In the flux-driven case, we observe $\Delta T < 0$ under the line and $\Delta T > 0$ over the line. On the other hand, in the temperature-driven case, we observe $\Delta F > 0$ under the line and $\Delta F < 0$ over the line.

It is widely believed that presheath region, existing between the sheath edge and the plasma, ions are accelerated to satisfy Bohm's criterion. In that situation, considering the horizontal line of $\tilde{\mathcal{M}} = 1$ in Figure 4.17, the transition occurs according to the boundary values of the flux or the temperature. In the flux-driven system, this transition is from smaller temperature-contrast states to larger states. In the temperature-driven system, it is from larger flux states to lower flux states.

Finally, we execute similar calculations for different values of the thermal diffusivity χ ($\chi = 1$ and $\chi = 100$) and show the results in Figures 4.18 and 4.19. Although the parameters where transitions occur (dashed lines) differ depending on the value of the χ, the features described above paragraphs are not changed.

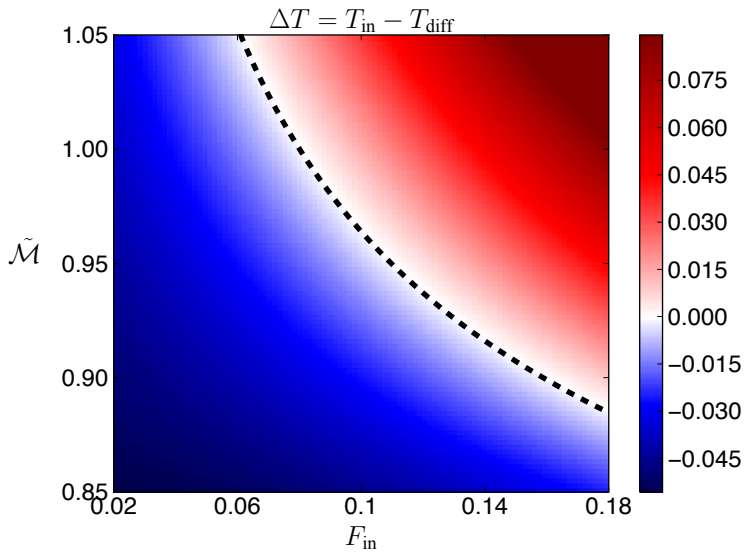

(a) Difference between the inside temperature Tin and that of linear diffusion case T_{diff} for the flux-driven system

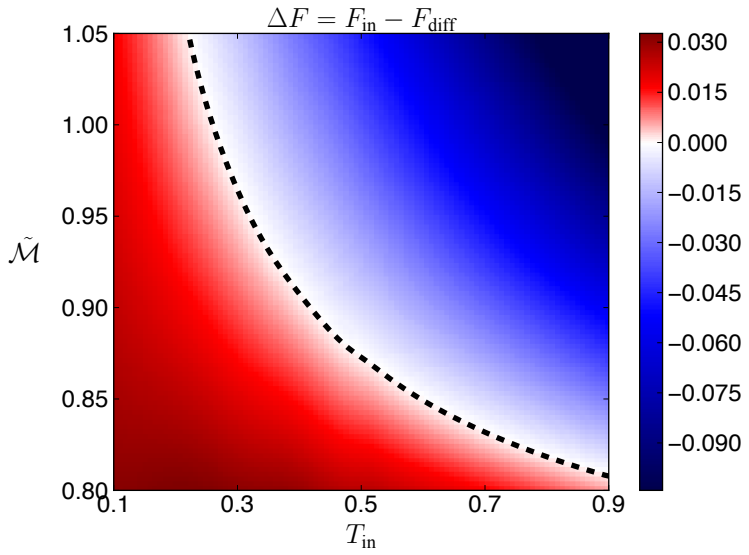

(b) Difference between the input flux Fin and that of linear diffusion case F_{diff} for the temperature-driven system

Figure 4.17: Comparison between sheath-diffusion coupling system and linear diffusion system with $\chi = 10$ (dashed lines: $\Delta F = 0$ or $\Delta T = 0$). In the flux-driven system, the transition from $\Delta T < 0$ to $\Delta T > 0$ occurs when F_{in} exceeds a threshold; and in the temperature-driven system, the transition from $\Delta F > 0$ to $\Delta F < 0$ occurs when T_{in} exceeds a threshold. Thresholds are determined by the value of $\tilde{\mathcal{M}}$.

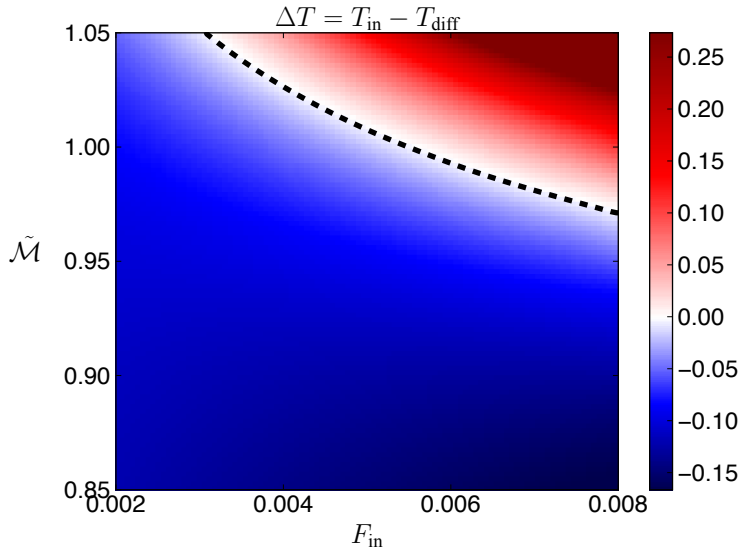

(a) Difference between the inside temperature Tin and that of linear diffusion case T_{diff} for the flux-driven system.

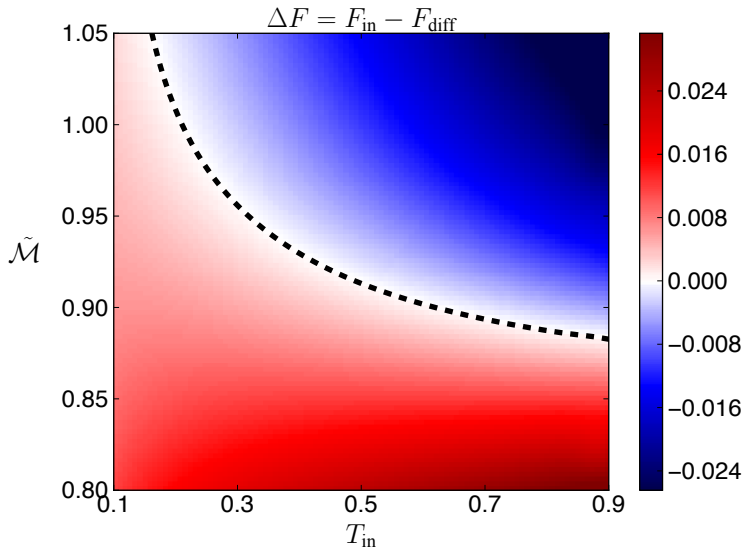

(b) Difference between the input flux Fin and that of linear diffusion case F_{diff} for the temperature-driven system

Figure 4.18: Comparison between sheath-diffusion coupling system and linear diffusion system with $\chi = 1$ (dashed lines: $\Delta F = 0$ or $\Delta T = 0$). Compared to Figure 4.17, the threshold lines move, but the features ($\Delta T \gtrless 0$, $\Delta F \gtrless 0$) do not change.

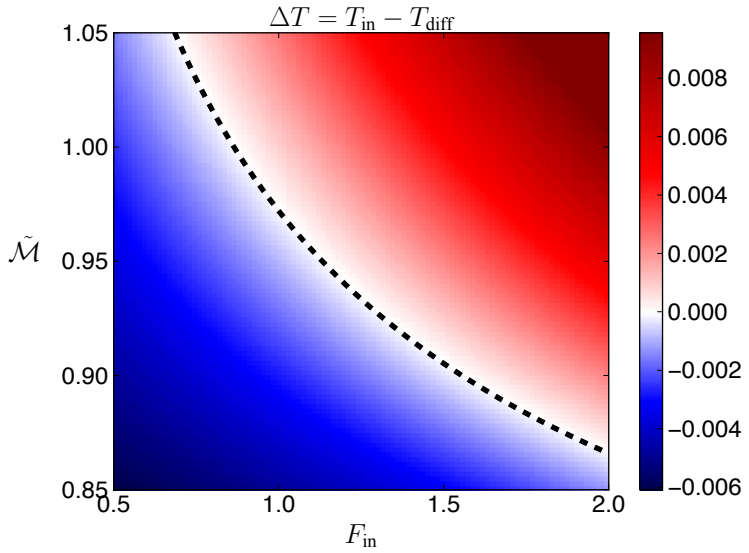

(a) Difference between the inside temperature Tin and that of linear diffusion case $T_{\rm diff}$ for the flux-driven system.

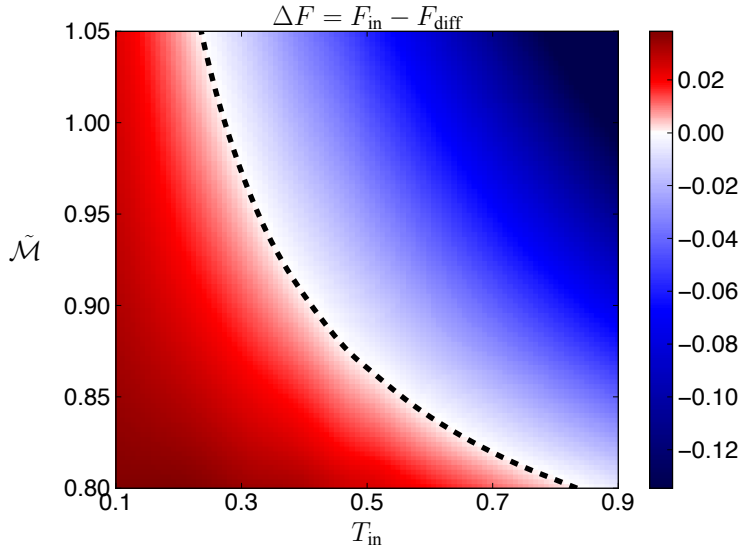

(b) Difference between the input flux Fin and that of linear diffusion case $F_{\rm diff}$ for the temperature-driven system

Figure 4.19: Comparison between sheath-diffusion coupling system and linear diffusion system with $\chi = 100$ (dashed lines: $\Delta F = 0$ or $\Delta T = 0$) Compared to Figure 4.17, the threshold lines move, but the features ($\Delta T \gtrless 0$, $\Delta F \gtrless 0$) do not change.

4.4 Conclusion

In this chapter, we have studied the thermal effect in sheath structures. At first, we have clarified that adiabatic ion temperature brings about two Sagdeev potentials and solution of Bohm's equation may bifurcate from one of them to the other. This bifurcation occurs at the singular point where the first-order derivatives of the Sagdeev potentials lose their Lipschitz continuities. We have classified the type of solutions based on the control parameters—the ion velocity and the temperature.

Next, we have investigated a non-adiabatic thermal effect. We have derived a second-order differential equation for the ion temperature including a thermal diffusion. There are two types of boundary conditions—flux-driven and temperature-driven systems. The self-organized presheath region accelerates ions, and its Mach number becomes one. Then, when the value of heat flux exceeds a threshold determined by the value of thermal diffusivity, the transition from smaller temperature-contrast states to larger states. In the temperature-driven system, the value of the boundary temperature exceeds a threshold, the transition from larger heat flux states to smaller states. This observation has an analogy to the result of a thermodynamical model of zonal flow [35, 87].

Chapter 5

Summary

We elucidated new aspects of ion acoustic waves by extending the classical model to larger systems including vortex and thermal effect. We were motivated by the facts that vortex characterizes dynamics of fluid motion and that we may view a self-organized structure in plasmas as a thermodynamical system.

In Chapter 2, we studied the vortex in ion acoustic wave equations. Since the KdV equation is one-dimensional systems, it does not have enough freedom for the existence of vorticity. Although the KP equation is two- or three-dimensional system, we showed that there are no vorticities. Moreover, we proved that not only the KP equation, the first-order terms of the reductive perturbation expansion, but also all of higher order terms are vortex-free. We also showed that thermal effect cannot produce vortexes. These facts indicate that the reductive perturbation method for the KP equation eliminates vortex. Then we focused on a minimal generalization of the KP equation with finite vorticity—the KPY equation. We showed that how the modification of reductive perturbation method avoids problems and allows the existence of vorticity.

We investigated the integrability of the KPY equation in Chapter 3. First, we proved that the system is non-integrable by the Painlevé test. This is because vortexes bring about an essential three-dimensionality. Next, we showed how the non-

integrability occurs by numerical simulation. The vortexes with small amplitudes twist the soliton periodically. Its frequency increases with increasing amplitude. When the amplitude of vortexes takes a large value, solitons do not get back to the initial state and break up into small structures. The transition is described by increasing Fourier components with high wave numbers and growing the vortex terms in the KPY equation.

In Chapter 4, we analyzed thermal effects in the electrostatic sheath. First, we found that the Bohm equation with the adiabatic ion temperature has two Sagdeev potentials. The first-order derivatives of them take the same value at the edge, and they lose the Lipschitz continuity at the point. Thus we may obtain solutions bifurcated from one of the Sagdeev potentials to the other one. We classified the type of solutions according to the values of the ion velocity and the ion temperature. Next, we included a non-adiabatic effect on the ion temperature—a heat flux. We solved a system composed of two differential equations for the ion temperature and the electrostatic potential. We took two types of boundary condition for the ion temperature equation; one is to control the heat flux, and the other is to control the temperature. In actual systems, the ion Mach number is fixed by the self-organized presheath, and the heat flux (not temperature) is controlled. In that condition, the temperature contrast takes a larger value than the linear diffusion state when the heat flux exceeds a threshold. This result indicates that the electrostatic sheath works as a barrier to a heat transport.

Appendix

A.1 Propagating solutions of KdV equation and KP equation

We derive propagating solutions of the KdV equation and the KP equation. We substitute $u(x,t) = f(x - vt) = f(\xi)$ into the KdV equation

$$\frac{\partial u}{\partial t} + \alpha u \frac{\partial u}{\partial x} + \beta \frac{\partial^3 u}{\partial x^3} = 0 \tag{A.1}$$

where α and β are constants, and obtain

$$-vf' + \alpha f f' + \beta f''' = 0 \tag{A.2}$$

with denoting $f' = \partial f / \partial \xi$. Integrating the equation we obtain

$$-vf + \frac{\alpha}{2} f^2 + \beta f'' = c_1 \tag{A.3}$$

with the integral constant c_1. Multiplying f', we can integrate the equation once more and obtain $-(v/2)f^2 + (\alpha/6)f^3 + (\beta/2)(f')^2 = c_1 f + c_2$ with the integral constant c_2. Assuming $c_1 = c_2 = 0$, this equation leads to

$$\sqrt{\frac{\beta}{v}} \int \frac{\mathrm{d}f}{f\sqrt{1 - (\alpha/3v)f}} = \int \mathrm{d}\xi \tag{A.4}$$

Calculating the integral, we obtain a solitary wave solution

$$u(x,t) = f(x - vt) = \frac{3v}{\alpha} \operatorname{sech}^2 \left[-\frac{1}{2} \sqrt{\frac{v}{\beta}} (x - vt + c) \right], \tag{A.5}$$

where c is the integral constant. Without assuming $c_1 = c_2 = 0$, we obtain cnoidal solutions (Jacobi elliptic functions), firstly derived by Korteweg and de Vries [41].

Next we calculate propagating solution of the two-dimensional KP equation

$$\frac{\partial}{\partial x}\left(\frac{\partial u}{\partial t}+\alpha\frac{\partial u}{\partial x}+\beta\frac{\partial^3 u}{\partial x^3}\right)+\gamma\frac{\partial^2 u}{\partial y^2}=0. \tag{A.6}$$

Substituting the expression $u(x,y,t)=f(x+ky-vt)=f(\xi)$, we obtain $(-vf'+\alpha ff'+\beta f''')'+\gamma k^2 f''=0$. The integration leads to $(-v+\gamma k^2)f'+\alpha ff'+\beta f'''=c_0$ with the integral constant c_0. Assuming $c_0=0$ and putting $\tilde{v}=v-\gamma k^2$, we obtain $-\tilde{v}f'+\alpha ff'+\beta f'''=0$, which is identified with the equation (A.2). Thus we may follow the calculation and obtain a solution

$$u(x,y,t)=\frac{3(v-\gamma k^2)}{\alpha}\operatorname{sech}^2\left[-\frac{1}{2}\sqrt{\frac{v-\gamma k^2}{\beta}}(x+ky-vt+c)\right]. \tag{A.7}$$

We remark that a propagating solution also exists for the three-dimensional KP equation

$$\frac{\partial}{\partial x}\left(\frac{\partial u}{\partial t}+\alpha\frac{\partial u}{\partial x}+\beta\frac{\partial^3 u}{\partial x^3}\right)+\gamma\frac{\partial^2 u}{\partial y^2}+\delta\frac{\partial^2 u}{\partial z^2}=0. \tag{A.8}$$

Calculating same as the two-dimensional KP equation, we obtain

$$u(x,y,z,t)=\frac{3(v-\gamma k^2-\delta l^2)}{\alpha}\operatorname{sech}^2\left[-\frac{1}{2}\sqrt{\frac{v-\gamma k^2-\delta l^2}{\beta}}(x+ky+lz-vt+c)\right], \tag{A.9}$$

However, that is not a soliton solution, since the three-dimensional KP equation is not integrable.

The difference between three-dimensional KP equation and the former two equations is in the existence of multiple soliton solutions. The KdV equation and the two-dimensional KP equation have N-soliton solutions which are expressed by eigenvalues in the inverse scattering transform (IST) method. However, the three-dimensional KP equation does not have three-soliton solutions [48].

A.2 Brief introduction to Sato theory and the KP hierarchy

As described in Section 1.2, Lax's formulation expand the IST method for the KdV equation to other equations. Lax's formulation also reveals "symmetries" of soliton equations. We may find an infinite number of linear operators A_n $(n = 1, 2, \ldots)$ which conserves eigenvalues of L (λ satisfying $L\psi = \lambda\psi$) under the time-evolution $\partial_{t'}\psi = A'\psi$. For the KdV equation, A_n can be defined with pseudo-differential operators ∂_x^j (j may be negative) as $A_n = (L^{n/2})^+$. Here, $L^{n/2}$ satisfy $(L^{n/2})^2 = L^n = (-\partial_x^2 + u)^n$ and $(L^{n/2})^+$ is the non-negative part of $L^{n/2}$. Thus, the operator L of the KdV equation has an infinite number of "times" t_n and operators A_n. Moreover, $\partial_{t_n}\partial_{t_m}L = \partial_{t_m}\partial_{t_n}L$ is satisfied, and thus the KdV equation has an infinite number of symmetries (momentum maps associated with the times). We obtain $\partial_{t_1}L = [A_1, L] = \partial_x L$ and $A = A_3$, thus t_1 is nothing but the coordinate x, and t_3 is the time of the original KdV equation. The set of Lax equations for t_n, $\partial_t L = [A_n, L]$, is called the *KdV hierarchy*.

Sato [65] used a pseudo-differential operator $W = \partial_x + \sum_{j=1}^{\infty} w_j \partial_x^{-j}$ and defined $L = W\partial_x W^{-1} = \partial_x + u_2\partial^{-1} + u_3\partial^{-2} + \cdots$. This procedure makes solving the scattering problem $L\psi = \lambda\psi$ and calculation of $A_n = (L^n)^+$ easily as $\partial_x(W^{-1}\psi) = \lambda(W^{-1}\psi)$ and $A_n = (W\partial_x^n W^{-1})^{-1}$. Lax equations $\partial_{t_n}L = [A_n, L]$, which are equivalent to the Sato equation $\partial_{t_n}W = A_n W - W\partial_x^n$, is a set of equations with an infinite number of functions u_j (or w_j) and variables t_n. From the terms of $n = 1$, we obtain $\partial_{t_1}L = \partial_x L$, and thus we may consider $t_1 = x$ same as the KdV hierarchy. Adjusting the terms of $n = 2, 3$, we obtain the equation for u_2,

$$\frac{\partial}{\partial x}\left(4\frac{\partial u_2}{\partial t_3} - 12u_2\frac{\partial u_2}{\partial x} - \frac{\partial^3 u_2}{\partial x^3}\right) - 3\frac{\partial^2 u_2}{\partial t_2^2} = 0. \tag{A.10}$$

This is nothing but the KP equation ($t_2 = y$, $t_3 = t$). Thus, the set of Lax equations (Sato equations) is called the *KP hierarchy*. We can obtain the KdV hierarchy and some of the hierarchies of soliton equations (such as the Boussinesq equation and the coupled KdV equation) by a procedure called *reduction*.

A.3 Hierarchy of three-dimensional fluid flow

We give a brief review of a significant role of vorticity in the context of noncanonical Hamiltonian formalism [51] and Clebsch representation [85] for ideal fluids.

A.3.1 Noncanonical Poisson structure and Casimir invariant

A generalized Hamiltonian equation of motion is written as

$$\frac{\partial F(u)}{\partial t} = \{F, H\}, \tag{A.11}$$

where F is a functional of a state vector $u \in X$ (X is a Hilbert space and we call phase space), H is a Hamiltonian, and $\{\ ,\ \}$ is a Poisson bracket. A Poisson bracket is a anti-symmetric bilinear operator satisfying the Jacobi identity $\{\{E, F\}, G\} + \{\{F, G\}, E\} + \{\{G, E\}, F\} = 0$. When a Poisson bracket may be written as $\{F, G\} = \langle \partial_u F, \mathcal{J}\partial_u G\rangle$, where $\langle\ ,\ \rangle$ is the inner product of X and $\partial_u F$ is the gradient of F, we call $\mathcal{J}$ a Poisson operator. A simple example is the Hamiltonian equation of motion for a particle; X is the space of position q and momentum p and the Poisson bracket is $\{F, G\} = \partial_q F \partial_p G - \partial_p F \partial_q G$.

A Poisson bracket $\{\ ,\ \}$ (or a Poisson operator $\mathcal{J}$) is called noncanonical if it has nontrivial kernels (a bracket without nontrivial kernels is called canonical). If a nontrivial kernel can be written by $\partial_u C$ ($\{C,\ \} = 0$, $\mathcal{J}\partial_u C = 0$) with a certain functional C, C is a constant of motion: $\partial C/\partial t = \{C, H\} = 0$. Such functional is called *Casimir invariant*. The significant feature of Casimir invariants is that they are conserved with *arbitrary* Hamiltonian. Thus Casimir invariants foliate phase spaces X and restrict the dynamical orbits to super-surfaces determined by values of Casimir invariants (called *Casimir leaves*) [89].

The Poisson operator for ideal fluids is written as

$$\mathcal{J} = \begin{pmatrix} 0 & -\nabla\cdot \\ -\nabla & -\rho^{-1}(\nabla \times \boldsymbol{u})\times \end{pmatrix}, \tag{A.12}$$

where the state vector is $u = (\rho, \boldsymbol{u})$. The Hamiltonian is the sum of the kinetic and internal energies: $H = \int (\rho|\boldsymbol{u}|^2/2 + \rho\mathcal{E}(\rho))\,\mathrm{d}^3x$. In the three-dimensional system (x, y, z), this bracket has two independent Casimir invariants; one is the total mass $\int \rho\,\mathrm{d}^3x$ and the other is the helicity

$$\int \boldsymbol{u} \cdot (\nabla \times \boldsymbol{u})\,\mathrm{d}^3x. \tag{A.13}$$

In the two-dimensional system (x, y), since $\boldsymbol{u} \cdot (\nabla \times \boldsymbol{u}) = 0$, the helicity is trivialized. Instead of the helicity, the generalized enstrophy

$$\int \rho f(\omega/\rho)\,\mathrm{d}^2x \tag{A.14}$$

$(\omega = (\nabla \times \boldsymbol{u}) \cdot \boldsymbol{e}_z)$ is conserved as a Casimir invariant.

When the value of vorticity is (globally) zero, both of the helicity and the generalized enstrophy become trivial. In that case, a new Casimir invariant

$$\int \boldsymbol{u} \cdot \boldsymbol{c}\,\mathrm{d}^nx, \tag{A.15}$$

where $n = 1, 2, 3$ is the spatial dimension and $\boldsymbol{c}$ is an arbitrary divergence-free vector, emerges due to the change of the Poisson bracket structure [89]:

$$\mathcal{J}' = \begin{pmatrix} 0 & -\nabla\cdot \\ -\nabla & 0 \end{pmatrix}. \tag{A.16}$$

Thus, we can say that a system without vorticity—including the KdV equation and the KP equation—resides on a "singular" Casimir leaf.

A.3.2 Clebsch representation and epi-two-dimensional flow

A (generalized) Clebsch representation for an n-dimensional vector field $\boldsymbol{u}$ is given by

$$\boldsymbol{u} = \nabla\phi + \sum_{i=1}^{n-1} \alpha_i \nabla\beta_i, \tag{A.17}$$

where ϕ, α_i, β_i are scalar function [85]. In the context of generalized Hamiltonian formalism, the Clebsch representation gives a transformation from noncanonical variables $(\rho, \boldsymbol{u})$ to canonical variables.

Let us consider the three-dimensional space and that $\boldsymbol{u}$ is a rotation-free vector field ($\nabla \times \boldsymbol{u} = 0$) and $\boldsymbol{v}$ is a vector field satisfying the condition $\boldsymbol{v} \cdot \nabla \times \boldsymbol{v} = 0$. Therefore the helicity of the field $\boldsymbol{u} + \boldsymbol{v}$ vanishes under a boundary condition eliminating boundary terms (such as the periodic boundary condition):

$$\int (\boldsymbol{u} + \boldsymbol{v}) \cdot \nabla \times (\boldsymbol{u} + \boldsymbol{v}) \, \mathrm{d}^3 x = \int \boldsymbol{u} \cdot \nabla \times \boldsymbol{v} \, \mathrm{d}^3 x = \int (\nabla \times \boldsymbol{u}) \cdot \boldsymbol{v} \, \mathrm{d}^3 x = 0. \quad \text{(A.18)}$$

From the knowledge of differential geometry, we can (locally) express these fields as $\boldsymbol{u} = \nabla\phi$ and $\boldsymbol{v} = \alpha\nabla\beta$. Compared with the equation (A.17), $\boldsymbol{u}+\boldsymbol{v} = \nabla\phi+\alpha\nabla\beta$ is the Clebsch representation of a two-dimensional vector field. However, we may see the field in the three-dimensional system. Such field is called *epi-two-dimensional flow* [88]. Epi-two-dimensional flow is certainly three-dimensional, whereas it conserves the generalized enstrophy and does not have a finite value of helicity. It is a class standing between the vortex-free flows $\nabla\phi$ and the general three-dimensional flows $\nabla\phi + \alpha_1\nabla\beta_2 + \alpha_2\nabla\beta_2$.

A.4 Lipschitz continuity and uniqueness of differential equation

We start by considering a nonlinear ordinary differential equation

$$\frac{\mathrm{d}x}{\mathrm{d}t} = \sqrt{x}, \qquad x(0) = 0. \quad \text{(A.19)}$$

Since this is a separable equation, we can solve easily and obtain a solution $x = t^2/4$. This solution is only valid for $t \geq 0$. On the other hand, $x \equiv 0$ is also a solution of the equation (A.19). Thus, we can say that the solution *bifurcates* at the point $t = 0$.

This is because the right-hand-side of the equation (A.19) is not *Lipschitz continuous* at $x = 0$. We say that a function $f(x, t)$ is Lipschitz continuous on a region S, if there is a positive constant M such that $|f(x_1, t) - f(x_2, t)| \leq M|x_1 - x_2|$ for all $(x_1, t), (x_2, t) \in S$.

If $f(x,t)$ is a Lipschitz continuous function on a region S and $(x_0,t_0) \in S$, the initial value problem

$$\frac{\mathrm{d}x}{\mathrm{d}t} = f(x(t),t), \qquad x(t_0) = x_0 \tag{A.20}$$

has an unique solution $x(t)$ in the region S. For a proof, see e.g., Ref. [13]

Since $f(x) = \sqrt{x}$ is not Lipschitz continuous at $x = 0$, the uniqueness of solution is lost and two bifurcated solutions $x = t^2/4$ and $x = 0$ can exist.

References

[1] M. J. Ablowitz, A. Ramani, and H. Segur, "Nonlinear evolution equations and ordinary differential equations of Painlevè type," Lett. Nuovo Cimento **23**, 333–338 (1978).

[2] M. J. Ablowitz, A. Ramani, and H. Segur, "A connection between nonlinear evolution equations and ordinary differential equations of P-type. I," J. Math. Phys. **21**, 715–721 (1980).

[3] M. J. Ablowitz and J. Villarroel, "On the Kadomtsev–Petviashvili equation and associated constraints," Stud. Appl. Math. **85**, 195–213 (1991).

[4] M. Akbari-Moghanjoughi, "Effects of ion-temperature on propagation of the large-amplitude ion-acoustic solitons in degenerate electron-positron-ion plasmas," Phys. Plasmas **17**, 082315 (2010).

[5] J. E. Allen, "The plasma-sheath boundary: its history and Langmuir's definition of the sheath edge," Plasma Sources Sci. Technol. **18**, 014004 (2009).

[6] V. I. Arnold, *Mathematical Methods of Classical Mechanics*, 2nd ed., Graduate Texts in Mathematics, Vol. 60 (Springer, New York, 1989).

[7] G. Biondini, K.-I. Maruno, M. Oikawa, and H. Tsuji, "Soliton interactions of the Kadomtsev–Petviashvili equation and generation of large-amplitude water waves," Stud. Appl. Math. **122**, 377–394 (2009), arXiv:0903.5279.

[8] D. Bohm, "Minimum ionic kinetic energy for a stable sheath," in *The Characteristics of Electrical Discharges in Magnetic Fields*, edited by A. Guthrie and R. K. Wakerling (McGraw-Hill, New York, 1949) Chap. 3, pp. 77–86.

[9] J. V. Boussinesq, *Essai sur la theorie des eaux courantes*, Mémoires présentés par divers savants à l'Académie des sciences de l'Institut national de France, Vol. XXIII (Institut national de France, Paris, 1877).

[10] H. W. Broer, "KAM theory: The legacy of Kolmogorov's 1954 paper," Bull. Amer. Math. Soc. **41**, 507–522 (2004).

[11] T. Brugarino and A. M. Greco, "Integrating the Kadomtsev–Petviashvili equation in the $1 + 3$ dimensions via the generalised Monge–Ampère equation: An example of conditioned Painlevé test," in *Physics on Manifolds*, Mathematical Physics Studies, Vol. 15, edited by M. Flato, R. Kerner, and A. Lichnerowicz (Kluwer Academic Publishers, Dordrecht, Netherlands, 1994) pp. 337–345.

[12] F. F. Chen, *Introduction to Plasma Physics and Controlled Fusion*, 3rd ed. (Springer International Publishing, Switzerland, 2016).

[13] E. A. Coddington, *An Introduction to Ordinary Differential Equations* (Dover, New York, 1989).

[14] R. Conte, "Invariant Painlevé analysis of partial differential equations," Phys. Lett. A **140**, 383–390 (1989).

[15] R. Conte, "The Painlevé approach to nonlinear ordinary differential equations," in *The Painlevé Property: One Century Later*, CRM Series in Mathematical Physics, edited by R. Conte (Springer-Verlag, New York, 1999) pp. 77–180, arXiv:solv-int/9710020.

[16] R. M. Corless, "Is $W(x)$ elementary?" Math 498/990 Notes (1995).

[17] E. Date, M. Kashiwara, M. Jimbo, and T. Miwa, "Transformation groups for soliton equations," in *Non-Linear Integrable Systems: Classical Theory and Quantum Theory*, edited by M. Jimbo and T. Miwa (World Scientific, Singapore, 1983) pp. 39–119.

[18] F. Del Sordo and A. Brandenburg, "Vorticity production through rotation, shear and baroclinicity," Astron. Astrophys. **528**, A145 (2011), arXiv:1008.5281.

[19] L. A. Dickey, *Soliton Equations and Hamiltonian Systems*, 2nd ed., Advanced Series in Mathematical Physics, Vol. 26 (World Scientific, Singapore, 2003).

[20] V. S. Dryuma, "Analytic solution of the two-dimensional Korteweg–de Vries (KdV) equation," JETP Lett. **19**, 387–388 (1974).

[21] W.-s. Duan, "The Kadomtsev–Petviashvili (KP) equation of dust acoustic waves for hot dust plasmas," Chaos Solitons Fractals **14**, 503–506 (2002).

[22] L. Einkemmer and A. Ostermann, "A splitting approach for the Kadomtsev–Petviashvili equation," J. Comput. Phys. **299**, 716–730 (2015), arXiv:1407.8154.

[23] R. N. Franklin, "The plasma-sheath boundary region," J. Phys. D: Appl. Phys.

36, R309–R320 (2003).

[24] C. S. Gardner, J. M. Greene, M. D. Kruskal, and R. M. Miura, "Method for solving the Korteweg–de Vries equation," Phys. Rev. Lett. **19**, 1095–1097 (1967).

[25] T. S. Gill, N. S. Saini, and H. Kaur, "The Kadomstev–Petviashvili equation in dusty plasma with variable dust charge and two temperature ions," Chaos Solitons Fractals **28**, 1106–1111 (2006).

[26] W. D. Halford and M. Vlieg-Hulstman, "Korteweg–de Vries–Burgers equation and the Painlevé property," J. Phys. A: Math. Gen. **25**, 2375–2379 (1999).

[27] Y.-H. Ichikawa, T. Mitsuhashi, and K. Konno, "Contribution of higher order terms in the reductive perturbation theory. I. A case of weakly dispersive wave," J. Phys. Soc. Japan **41**, 1382–1386 (1976).

[28] E. Infeld, A. Senatorski, and A. A. Skorupski, "Decay of Kadomtsev–Petviashvili solitons," Phys. Rev. Lett. **72**, 1345–1347 (1994).

[29] E. Infeld, A. Senatorski, and A. A. Skorupski, "Numerical simulations of Kadomtsev–Petviashvili soliton interactions," Phys. Rev. E **51**, 3183–3191 (1995).

[30] M. Jimbo, M. D. Kruskal, and T. Miwa, "Painlevé test for the self-dual Yang–Mills equation," Phys. Lett. A **92**, 59–60 (1982).

[31] B. B. Kadomtsev and V. I. Petviashvili, "On the stability of solitary waves in weakly dispersing media," Sov. Phys. Dokl. **15**, 539–541 (1970).

[32] M. Kako and G. Rowlands, "Two-dimensional stability of ion-acoustic solitons," Plasma Phys. **18**, 165–170 (1976).

[33] B. C. Kalita and M. K. Kalita, "Modified Korteweg–de Vries solitons in a warm plasma with negative ions," Phys. Fluids B **2**, 674–676 (1990).

[34] C.-Y. Kao and Y. Kodama, "Numerical study of the KP equation for non-periodic waves," Math. Comput. Simulat. **82**, 1185–1218 (2012), arXiv:1004.0407.

[35] Y. Kawazura and Z. Yoshida, "Entropy production rate in a flux-driven self-organizing system," Phys. Rev. E **82**, 066403 (2010).

[36] Y. Kawazura and Z. Yoshida, "Comparison of entropy production rates in two different types of self-organized flows: Bénard convection and zonal flow," Phys. Plasmas **19**, 012305 (2012), arXiv:1109.1955.

[37] C. Klein and K. Roidot, "Fourth order time-stepping for Kadomtsev–Petviashvili and Davey–Stewartson equations," SIAM J. Sci. Comput. **33**, 3333–3356 (2011).

[38] C. Klein, C. Sparber, and P. Markowich, "Numerical study of oscillatory regimes in the Kadomtsev–Petviashvili equation," J. Nonlinear Sci. **17**, 429–470 (2007), arXiv:math-ph/0601025.

[39] K. Konno and Y.-H. Ichikawa, "A modified Korteweg de Vries equation for ion acoustic waves," J. Phys. Soc. Japan **37**, 1631–1636 (1974).

[40] K. Konno, T. Mitsuhashi, and Y.-H. Ichikawa, "Dynamical processes of the dressed ion acoustic solitons," J. Phys. Soc. Japan **43**, 669–674 (1977).

[41] D. J. Korteweg and G. de Vries, "On the change of form of long waves advancing in a rectangular canal, and on a new type of long stationary waves," Philos. Mag. Ser. 5 **39**, 422–443 (1895); reprinted in Philos. Mag. **91**, 1007–1028 (2011).

[42] M. D. Kruskal and P. A. Clarkson, "The Painlevé–Kowalevski and poly-Painlevé tests for integrability," Stud. Appl. Math. **86**, 87–165 (1992).

[43] I. Langmuir, "The interaction of electron and positive ion space charges in cathode sheaths," Phys. Rev. **33**, 954–989 (1929).

[44] P. D. Lax, "Integrals of nonlinear equations of evolution and solitary waves," Commun. Pure Appl. Math. **21**, 467–490 (1968).

[45] M.-m. Lin and W.-s. Duan, "The Kadomtsev–Petviashvili (KP), MKP, and coupled KP equations for two-ion-temperature dusty plasmas," Chaos Solitons Fractals **23**, 929–937 (2005).

[46] V. D. Lipovskii, "Hamiltonian structure of the Kadomtsev–Petviashvili-II equation in the class of decreasing Cauchy data," Funct. Anal. Appl. **20**, 282–291 (1986).

[47] K. E. Lonngren, "Ion acoustic soliton experiments in a plasma," Opt. Quantum Electron. **30**, 615–630 (1998).

[48] W.-X. Ma, "Comment on the $3+1$ dimensional Kadomtsev–Petviashvili equations," Commun. Nonlinear Sci. Numer. Simulat. **16**, 2663–2666 (2011).

[49] R. I. McLachlan and G. R. W. Quispel, "Splitting methods," Acta Numer. **11**, 341–434 (2002).

[50] T. Miwa, M. Jimbo, and E. Date, *Solitons: Differential Equations, Symmetries and Infinite Dimensional Algebras*, Cambridge Tracts in Mathematics, Vol. 135

(Cambridge University Press, Cambridge, 2000).

[51] P. J. Morrison, "Hamiltonian description of the ideal fluid," Rev. Mod. Phys. **70**, 467–521 (1998).

[52] M. Musette, "Painlevé analysis for nonlinear partial differential equations," in *The Painlevé Property: One Century Later*, CRM Series in Mathematical Physics, edited by R. Conte (Springer-Verlag, New York, 1999) pp. 517–572, arXiv:solv-int/9804003.

[53] Y. Nakamura, "Experiments on ion-acoustic solitons in plasmas," IEEE Trans. Plasma Sci. **PS-10**, 180–195 (1982).

[54] S. Nishibata, M. Ohnawa, and M. Suzuki, "Asymptotic stability of boundary layers to the Euler–Poisson equations arising in plasma physics," SIAM J. Math. Anal. **44**, 761–790 (2012).

[55] K. Nozaki, "Solitons as invariant tori in the perturbed nonlinear Schrödinger equation," Physica D **23**, 369–373 (1986).

[56] K. Nozaki and N. Bekki, "Chaotic solitons in a plasma driven by an rf field," J. Phys. Soc. Japan **54**, 2363–2366 (1985).

[57] Y. Ohno and Z. Yoshida, "Nonlinear ion acoustic waves scattered by vortexes," Commun. Nonlinear Sci. Numer. Simulat. **38**, 277–287 (2016), arXiv:1512.00289.

[58] Y. Ohta, J. Satsuma, D. Takahashi, and T. Tokihiro, "An elementary introduction to Sato theory," Prog. Theor. Phys. Suppl. **94**, 210–241 (1988).

[59] I. S. O'Keir and E. J. Parkes, "The derivation of a modified Kadomtsev–Petviashvili equation and the stability of its solutions," Phys. Scr. **55**, 135–142 (1997).

[60] J. Pedlosky, *Geophysical Fluid Dynamics*, 2nd ed. (Springer-Verlag, New York, 1987).

[61] W. H. Press, S. A. Teukolsky, W. T. Vetterling, and B. P. Flannery, *Numerical Recipes: The Art of Scientific Computing*, 3rd ed. (Cambridge University Press, 2007).

[62] K.-U. Riemann, "The Bohm criterion and sheath formation," J. Phys. D: Appl. Phys. **24**, 493–518 (1991).

[63] H.-y. Ruan, S.-y. Lou, and Y.-x. Chen, "Conformal invariant expansion and high-dimensional Painlevé integrable models," J. Phys. A: Math. Gen. **32**,

2719–2729 (1999).

[64] R. Z. Sagdeev, "Cooperative phenomena and shock waves in collisionless plasmas," in *Reviews of Plasma Physics*, Vol. 4, edited by M. A. Leontovich (Consultants Bureau, New York, 1966) pp. 23–91.

[65] M. Sato, "Soliton equations as dynamical systems on a infinite dimensional Grassmann manifolds," RIMS Kokyuroku **439**, 30–46 (1981).

[66] H. Schamel, "A modified Korteweg–de Vries equation for ion acoustic wavess due to resonant electrons," J. Plasma Phys. **9**, 377–387 (1973).

[67] A. Senatorski and E. Infeld, "Breakup of two-dimensional into three-dimensional Kadomtsev–Petviashvili solitons," Phys. Rev. E **57**, 6050–6055 (1998).

[68] P. C. Stangeby, *The Plasma Boundary of Magnetic Fusion Devices*, Series in Plasma Physics (IOP Publishing, Bristol, 2000).

[69] G. Strang, "On the construction and comparison of difference schemes," SIAM J. Numer. Anal. **5**, 506–517 (1968).

[70] S. G. Tagare, "Effect of ion temperature on propagation of ion-acoustic solitary waves of small amplitudes in collisionless plasma," Plasma Phys. **15**, 1247–1252 (1973).

[71] T. Takizuka and M. Hosokawa, "Particle simulation study of the effect of radial electric field on scrape-off layer plasma and sheath formation," Contrib. Plasma Phys. **40**, 471–477 (2000).

[72] T. Takizuka, K. Tani, M. Azumi, and K. Shimizu, "Particle simulation of divertor plasma," J. Nucl. Mater. **128–129**, 104–110 (1984).

[73] F. Tappert, "Improved Korteweg–de Vries equation for ion-acoustic waves," Phys. Fluids **15**, 2446–2447 (1972).

[74] S.-F. Tian and H.-Q. Zhang, "On the integrability of a generalized variable-coefficient Kadomtsev–Petviashvili equation," J. Phys. A: Math. Theor. **45**, 055203 (2012), arXiv:1112.1499.

[75] R. S. Tiwari and M. K. Mishra, "Ion-acoustic dressed solitons in a dusty plasma," Phys. Plasmas **13**, 062112 (2006).

[76] S. Togo, T. Takizuka, M. Nakamura, K. Hoshino, K. Ibano, T. L. Lang, and Y. Ogawa, "Simulation study of detached plasmas by using one-dimensional SOL-divertor fluid code with virtual divertor model," Contrib. Plasma Phys.

56, 729–735 (2016).

[77] S. Togo, T. Takizuka, M. Nakamura, K. Hoshino, and Y. Ogawa, "SOL-divertor plasma simulations introducing anisotropic temperature with virtual divertor model," J. Nucl. Mater. **463**, 502–505 (2015).

[78] M. Q. Tran, "Ion acoustic solitons in a plasma: A review of their experimental properties and related theories," Phys. Scr. **20**, 317–327 (1979).

[79] M. Q. Tran and P. J. Hirt, "The Korteweg–de Vries equation for a two component plasma," Plasma Phys. **16**, 617–621 (1974).

[80] H. Ur-Rehman, "The Kadomtsev–Petviashvili equation for dust ion-acoustic solitons in pair-ion plasmas," Chinese Phys. B **22**, 035202 (2013).

[81] H. Washimi and T. Taniuti, "Propagation of ion-acoustic solitary waves of small amplitude," Phys. Rev. Lett. **17**, 996–998 (1966).

[82] J. Weiss, "The Painlevé property for partial differential equations. II: Bäcklund transformation, Lax pair and the Schwarzian derivative," J. Math. Phys. **24**, 1405–1413 (1983).

[83] J. Weiss, M. Tabor, and G. Carnevale, "The Painlevé property for partial differential equations," J. Math. Phys. **24**, 522–526 (1983).

[84] G.-q. Xu and Z.-b. Li, "Symbolic computation of the Painlevé test for nonlinear partial differential equations using Maple," Comput. Phys. Commun. **161**, 65–75 (2004).

[85] Z. Yoshida, "Clebsch parameterization: Basic properties and remarks on its applications," J. Math. Phys. **50**, 113101 (2009).

[86] Z. Yoshida, *Nonlinear Science: The Challenge of Complex Systems* (Springer-Verlag, Berlin, Heidelberg, 2010).

[87] Z. Yoshida and S. M. Mahajan, "'Maximum' entropy production in self-organized plasma boundary layer: A thermodynamic discussion about turbulent heat transport," Phys. Plasmas **15**, 032307 (2008).

[88] Z. Yoshida and P. J. Morrison, "Epi-two-dimensional flow and generalized enstrophy," arXiv preprint (2016), arXiv:1604.02339.

[89] Z. Yoshida and P. J. Morrison, "Hierarchical structure of noncanonical Hamiltonian systems," Phys. Scr. **91**, 024001 (2016), arXiv:1410.2936.

[90] Z. Yoshida and H. Yamada, "Dissipative structure of plasmas: remarks on elec-

trostaic potential distribution in plasmas," in *Proceedings of the 13th Sapporo Symposium on Partial Differential Equations*, Hokkaido University Technical Report Series in Mathematics, Vol. 8, edited by K. Kubota (Department of Mathematics, Hokkaido University, 1988) pp. 21–28.

[91] N. J. Zabusky and M. D. Kruskal, "Interaction of 'solitons' in a collisionless plasma and the recurrence of initial states," Phys. Rev. Lett. **15**, 240–243 (1965).

[92] V. E. Zakharov and L. D. Faddeev, "Korteweg–de Vries equation: A completely integrable Hamiltonian system," Funct. Anal. Appl. **5**, 280–287 (1971).

[93] V. E. Zakharov and A. B. Shabat, "Exact theory of two-dimenstional self-focusing and one-dimensional self-modulation waves in nonlinear media," Sov. Phys. JETP **34**, 62–69 (1972).

[94] V. E. Zakharov and A. B. Shabat, "A scheme for integrating the nonlinear equations of mathematical physics by the method of the inverse scattering problem. I," Funct. Anal. Appl. **8**, 226–235 (1974).

List of Publications

Peer-reviewed Article

1. Yuji Ohno and Zensho Yoshida: "Nonlinear ion acoustic waves scattered by vortexes," Communications in Nonlinear Science and Numerical Simulation **38** (2016) 277–287 [doi:10.1016/j.cnsns.2016.02.018, arXiv:1512.00289]

Oral Presentation

1. Yuji Ohno, Zensho Yoshida, and Hosam N. Abdelrazek: "Ion acoustic soliton with finite vortex," Plasma Conference 2014, 20pD2-1, Toki Messe (2014.11.20)

2. 大野裕司，吉田善章：「渦をもつ非線形イオン音波」日本物理学会第 70 回年次大会，21pBH-11，早稲田大学 (2015.03.21)

3. 大野裕司，吉田善章：「非線形イオン音波における渦と非可積分性」日本物理学会 2015 年秋季大会，17aCW-5，関西大学 (2015.09.17)

4. 大野裕司，吉田善章：「渦をもつ非線形イオン音波の可積分性に関する数値的検証」日本流体力学会 年会 2015，東京工業大学 (2015.09.27)

5. 大野裕司，吉田善章：「渦をもつ非線形イオン音波の非可積分性について」RIMS 研究集会『非線形波動現象の数理に関する最近の進展』，京都大学数理解析研究所 (2015.10.16)

6. 大野裕司, 吉田善章:「渦によって散乱される非線形イオン音波における状態遷移について」日本物理学会第 71 回年次大会, 19aBU-6, 東北学院大学 (2016.03.19)

7. 大野裕司, 吉田善章:「静電ポテンシャル構造の熱的効果による分岐について」日本物理学会 2016 年秋季大会, 15aKC-11, 金沢大学 (2016.09.15)

8. 大野裕司, 吉田善章:「熱拡散と相互作用するシースの性質について」日本物理学会第 72 回年次大会, 20aC33-8, 大阪大学（発表予定）

Poster Presentation

1. Yuji Ohno: "Ion Acoustic Solitary Waves with Finite Vorticity," Joint ICTP–IAEA College on Advanced Plasma Physics, ICTP, Trieste, Italy (2014.8.18–29)

2. Yuji Ohno and Zensho Yoshida: "Chaos of nonlinear ion acoustic waves with vorticity," 25th International Toki Conference (ITC-25), P2-28, Ceratopia Toki, Toki-city, Gifu, Japan (2015.11.3–6)

Award

1. 大野裕司:「日本物理学会第 70 回年次大会 領域 2 学生優秀発表賞」, 2015 年 3 月

Acknowledgments

I would like to express my sincerest appreciation to many people for their kind supports.

First of all, I would like to express my deepest gratitude to my supervisor Professor Zensho Yoshida. It has been over five years since entering the laboratory when I was an undergraduate student. He has given me a lot of instructions and remarks. I have been tried to acquire a wider perspective during my work with him as much I could. I would never complete this dissertation without him.

I sincerely appreciate Dr. Yohei Kawazura and Associate Professor Masaki Nishiura. Dr. Kawazura helped my graduation thesis and master's thesis on studies of drift wave turbulences. He also gave me a lot of helpful advice after I entered the doctoral course and started to study ion acoustic waves. Professor Nishiura has given me many fruitful comments from the viewpoint of experiments.

I also would like to express my gratitude to members of the dissertation committee, Professor Yoshida, Professor Nishiura, Professor Naoaki Bekki, Professor Yuichi Ogawa, and Professor Kojiro Suzuki. They provided many helpful comments for improving my work.

I appreciate many elders and betters of the laboratory, former Associate Professor Masaru Furukawa, Mr. Junji Morikawa, Dr. Haruhiko Saitoh, Dr. Yoshihisa Yano, Dr. Francesco Volponi, Dr. Yuta Kaneko, Dr. Shingo Emoto, Dr. Naoki Kenmochi, and Dr. Hosam Abd El-Razek. My life in the graduate school has been supported

by them.

I express my thank to Ms. Kyoko Kitayama for her kind hospitality. She always encourages laboratory members and helps our paperwork.

I thank Mr. Hamdi Abdelhamid and Mr. Naoki Sato. A lot of discussion with them improves my understanding of plasma physics and surrounding mathematics. I also thank all of the current and past students of the laboratory and hope their success.

Finally, I would like to express my sincere appreciation to my parents. I could finish my work on this dissertation with their kind support and encouragement.

Yuji Ohno